Redox Biology 36 (2020) 101601

Contents lists available at ScienceDirect

Redox Biology

journal homepage: www.elsevier.com/locate/redox

An effective inactivant based on singlet oxygen-mediated lipid oxidation implicates a new paradigm for broad-spectrum antivirals

Lei Zeng[a,b,c,1], Meng-Di Wang[a,b,c,1], Sheng-Li Ming[a,b,c,1], Guo-Li Li[a,b,c], Peng-Wei Yu[a,b,c], Yan-Li Qi[a,b,c], Da-Wei Jiang[a,d], Guo-Yu Yang[a,b,c,**], Jiang Wang[a,b,c,***], Bei-Bei Chu[a,b,c,d,*,2]

[a] College of Animal Sciences and Veterinary Medicine, Henan Agricultural University, Zhengzhou, Henan Province, PR China
[b] Key Laboratory of Animal Biochemistry and Nutrition, Ministry of Agriculture and Rural Affairs, Henan Agricultural University, Zhengzhou, Henan Province, PR China
[c] Henan Provincial Key Laboratory of Animal Growth and Development Regulation, The Education Department of Henan Provence, Henan Agricultural University, Zhengzhou, Henan Province, PR China
[d] National Center for International Research, Ministry of Science and Technology, Henan Agricultural University, Zhengzhou, Henan Province, PR China

ARTICLE INFO

Keywords:
Singlet oxygen
Lipid oxidation
Membrane fusion
Inactivated virus vaccine
Immunization
Broad-spectrum antivirals

ABSTRACT

Emerging viral pathogens cause substantial morbidity and pose a severe threat to health worldwide. However, a universal antiviral strategy for producing safe and immunogenic inactivated vaccines is lacking. Here, we report an antiviral strategy using the novel singlet oxygen ($^1O_2$)-generating agent LJ002 to inactivate enveloped viruses and provide effective protection against viral infection. Our results demonstrated that LJ002 efficiently generated $^1O_2$ in solution and living cells. Nevertheless, LJ002 exhibited no signs of acute toxicity in vitro or *in vivo*. The $^1O_2$ produced by LJ002 oxidized lipids in the viral envelope and consequently destroyed the viral membrane structure, thus inhibiting the viral and cell membrane fusion necessary for infection. Moreover, the $^1O_2$-based inactivated pseudorabies virus (PRV) vaccine had no effect on the content of the viral surface proteins. Immunization of mice with LJ002-inactiviated PRV vaccine harboring comparable antigen induced more neutralizing antibody responses and efficient protection against PRV infection than conventional formalin-inactivated vaccine. Additionally, LJ002 inactivated a broad spectrum of enveloped viruses. Together, our results may provide a new paradigm of using broad-spectrum, highly effective inactivants functioning through $^1O_2$-mediated lipid oxidation for developing antivirals that target the viral membrane fusion process.

1. Introduction

Emerging viral pathogens are a constant and prominent threat to health worldwide. Viral infections in animals cause devastating economic losses, severely affect animal welfare, and have potential environmental and global biodiversity consequences [1]. Moreover, animals are thought to be the major sources of human zoonotic infections, and 75% of all emerging infectious diseases are considered to be caused by animals [2]. Pseudorabies virus (PRV) is an acute infectious disease characterized by respiratory symptoms, fever, and reproductive and nervous system diseases in livestock such as pigs, cattle, goats, and many wild animals [3]. One case of human endophthalmitis has been reported to be caused by PRV infection [4]. The pig industry in China has suffered enormous economic losses because of the reemergence and large-scale prevalence of PRV variants since 2011 [5]. African swine fever virus (ASFV) is the causative agent of a highly contagious hemorrhagic disease affecting wild boars and domestic pigs, with mortality rates approaching 100%. ASFV has spread into many countries in Africa, Europe, South America, the Caribbean region, and Asia, especially Russia and China [6–8]. Because no vaccine or antiviral strategy it is available, more than 30 million pigs were culled during 2018–2019, translating to estimated economic losses of $2 billion in swine production worldwide [9]. Furthermore, the recent outbreaks of severe acute respiratory syndrome, Ebola virus, Zika virus, and novel influenza strains with pandemic potential are examples of zoonotic pathogens causing different types of diseases representing major global

* Corresponding author. College of Animal Sciences and Veterinary Medicine, Henan Agricultural University, Zhengzhou, Henan Province, PR China.
** Corresponding author. College of Animal Sciences and Veterinary Medicine, Henan Agricultural University, Zhengzhou, Henan Province, PR China.;
*** Corresponding author. College of Animal Sciences and Veterinary Medicine, Henan Agricultural University, Zhengzhou, Henan Province, PR China.;
E-mail addresses: haubiochem@163.com (G.-Y. Yang), wangjiang_hau@hotmail.com (J. Wang), chubeibei_hau@hotmail.com (B.-B. Chu).
[1] These authors contributed equally to this work.
[2] Lead contact.

https://doi.org/10.1016/j.redox.2020.101601
Received 3 January 2020; Received in revised form 16 May 2020; Accepted 2 June 2020
Available online 08 June 2020

public health issues [10].

Immunization is the most important and cost-effective strategy to protect animals from these emerging viral diseases. Besides improving animal health, immunization also substantially enhances public health by preventing the occurrence of several zoonotic diseases [11]. Thus, there is a dire need to develop vaccine candidates and novel agents in response to new viral pathogens. Inactivated virus vaccines circumvent the need to identify relevant antigens, and they contain many immunogenic epitopes to evoke effective virus-specific immune responses. Moreover, inactivated virus vaccines can be quickly produced from purified viruses through chemical inactivation methods. Unfortunately, a general method for producing safe and immunogenic inactivated vaccines is lacking. Conventionally, formalin has been extensively used to inactivate viruses in the manufacture of vaccines [12]. However, formalin treatment not only generates carbonyl groups on vaccine antigens, thus inducing harmful and undesirable T helper type 2 biased immune responses [13], but also causes structural damage to B-cell epitopes [14] and introduces carcinogenesis [15]. Owing to its drawbacks, research focus has shifted towards aziridin derivatives acting on nucleic acids; these derivatives are highly reliable in inactivating various DNA and RNA viruses. However, these aziridine derivatives are also highly toxic and unstable [16,17]. Alternative virus inactivation methods, such as ultraviolet light, gamma radiation, and heating, all have the drawbacks of the various limitations mentioned above [18,19].

$^1O_2$ is a reactive oxygen species with well-established roles in programmed cell death signaling or acclimation processes in plants and microorganisms [20,21]. The high reactivity of $^1O_2$ also results in the production of reaction products such as oxidized lipids, which can function as second messengers that mediate signal transduction and activate redox-sensitive transcription factors [22,23]. In mammals, $^1O_2$ plays a pathophysiological role in regulating vascular tone and blood pressure under inflammatory conditions [24]. Chemical generation of $^1O_2$ requires light activation of photosensitizer (such as porphyrins, chlorines and thiazolidine) into the triplet state and transfers the energy to O_2, thus forming $^1O_2$, a highly reactive species with applications in blood sterilization, herbicides, insecticides, wastewater treatment, fine chemical synthesis, and photodynamic therapy [25,26]. Recently, the broad-spectrum antiviral compound LJ001 has been shown to inhibit infection with enveloped viruses by modifying phospholipids in the lipid bilayer via the production of $^1O_2$ [27]. However, unfortunately, the use of LJ001 and its structural homologs (JL122 and JL118) in a murine lethal challenge model of viruses is impractical, owing to the lack of light exposure inside the body to activate the compound [28]. Whether $^1O_2$-based lipid modification can be used to inactivate viruses and induce immune responses remains unknown.

Lipids are a major component of membrane-enveloped viruses, which play important roles in merging two initially distinct lipid bilayers into a single lipid bilayer, thus enabling fusion of viral and cell membranes for viral entry [29]. $^1O_2$ readily oxidizes lipids containing carbon-carbon double bonds and introduces hydroperoxy group into them [26], thus specially causing changes in membrane properties. On the basis of these earlier observations, we hypothesized that $^1O_2$ treatment might provide an attractive method to generate effective inactivated virus vaccines. Furthermore, because viral lipid membranes are not encoded by the viral genome, such inactivation strategies would also probably increase the barrier to viral variation-induced resistance.

Here, we synthesized LJ002, the structural analogue of LJ001, an ethyl thiazolidine derivative, with the objective of exploring a novel $^1O_2$-based virus inactivation strategy, as a putative alternative to current agents such as formalin for the preparation of inactivated vaccines. Our results demonstrate that LJ002 efficiently generates $^1O_2$ in solution and living cells. The produced $^1O_2$ oxidizes lipids in the viral envelope, thus leading to destruction of the viral membrane structure and inhibition of the membrane fusion necessary for cell infection. Moreover, the $^1O_2$-based inactivated PRV vaccine has no effect on the viral surface protein content and confers a stronger neutralizing antibody response than conventional formalin-inactivated PRV vaccine, thereby providing more efficient protection against lethal-dose PRV challenge. In addition, the inactivation mediated by $^1O_2$ is effective against different families of enveloped viruses, thus demonstrating the ability to generate inactivated virus vaccines with greater potency than vaccines produced by current inactivation techniques.

2. Materials and methods

2.1. Materials

We obtained TRIzol Reagent (D9108B) and SYBR Premix Ex Taq (RR420A) from TaKaRa; a Cell Counting Kit-8 (CCK-8, ZP328) from Zoman Bio (Beijing, China); a malondialdehyde (MDA) test kit (A003-4) from Jian Cheng (Nanjing, China); mouse monoclonal anti-actin (A1978) from Sigma; Lycopene (HY–N0287) and methylene blue (HY-14536) from MedChemExpress; Singlet Oxygen Sensor Green (S36002) from Invitrogen; deuterium oxide (D_2O, D113904) from Aladdin (Shanghai, China). Anti-glycoprotein E (gE) [30] was a gift from Professor Ke-Gong Tian (Henan Agricultural University, China). Antisera against PRV glycoprotein B (gB) were generated by immunization of mice with purified recombinant gB. Horseradish-peroxidase-conjugated donkey anti-mouse IgG (715-035-150) and anti-rabbit IgG (711-035-152) antibodies were from Jackson ImmunoResearch Laboratories; anti-mouse IgG antibody labeled with Alexa Fluor 488 (A21429) was from Thermo Fisher Scientific. The antibodies described above were used at dilutions of 1:500 for immunofluorescence staining and 1:1,000 for immunoblotting. MDA (BWQ7504-2016) was from Beijing Northern Weiye Institute of Metrology and Technology. LJ002 and LJ001 were synthesized as previously described [27].

2.2. Cells and viruses

PK-15, Vero, MARC-145, and HeLa cells were grown in monolayers at 37 °C under 5% CO_2. All cells were cultured in DMEM (10566–016, GIBCO), supplemented with 10% FBS (10099141C, GIBCO), 100 units/mL penicillin, and 100 μg/mL streptomycin sulfate (B540732, Sangon).

PRV-GFP and PRV-QXX were used as previously described [31,32]. PRV HN1201 [33] was a gift from Professor Ke-Gong Tian (Henan Agricultural University, China). Vesicular stomatitis virus (VSV)-GFP, Newcastle disease virus (NDV)-GFP, influenza virus (H1N1 PR8), and Sendai virus (SeV) [34] were gifts from Yong-Tao Li (Henan Agricultural University, China). Porcine reproductive and respiratory syndrome virus (PRRSV)-GFP [35] was a gift from Professor En-Min Zhou (Northwest A&F University, China).

2.3. Cell viability assays

Cells were seeded into 96-well plates with 0.8×10^4 cells/well for the indicated time periods, and cell viability was determined with CCK-8 assays according to the manufacturer's instructions. The absorbance at 450 nm was detected with a microplate reader (Awareness Technology Inc.).

2.4. Half maximal inhibitory concentration (IC50) assays

The IC50 values for LJ002 in PK-15 cells were determined after 48 h of treatment. Briefly, 1×10^4 cells were seeded into 96-well plates and treated with various LJ002 concentrations (0, 20 nM, 60 nM, 0.2 μM, 0.6 μM, 2 μM, 6 μM, 20 μM, and 60 μM) for 48 h, and CCK-8 survival assays were then carried out to evaluate cell viability under different drug concentrations. A graph of viability versus drug concentration was constructed in Prism 7 to calculate the IC50 values.

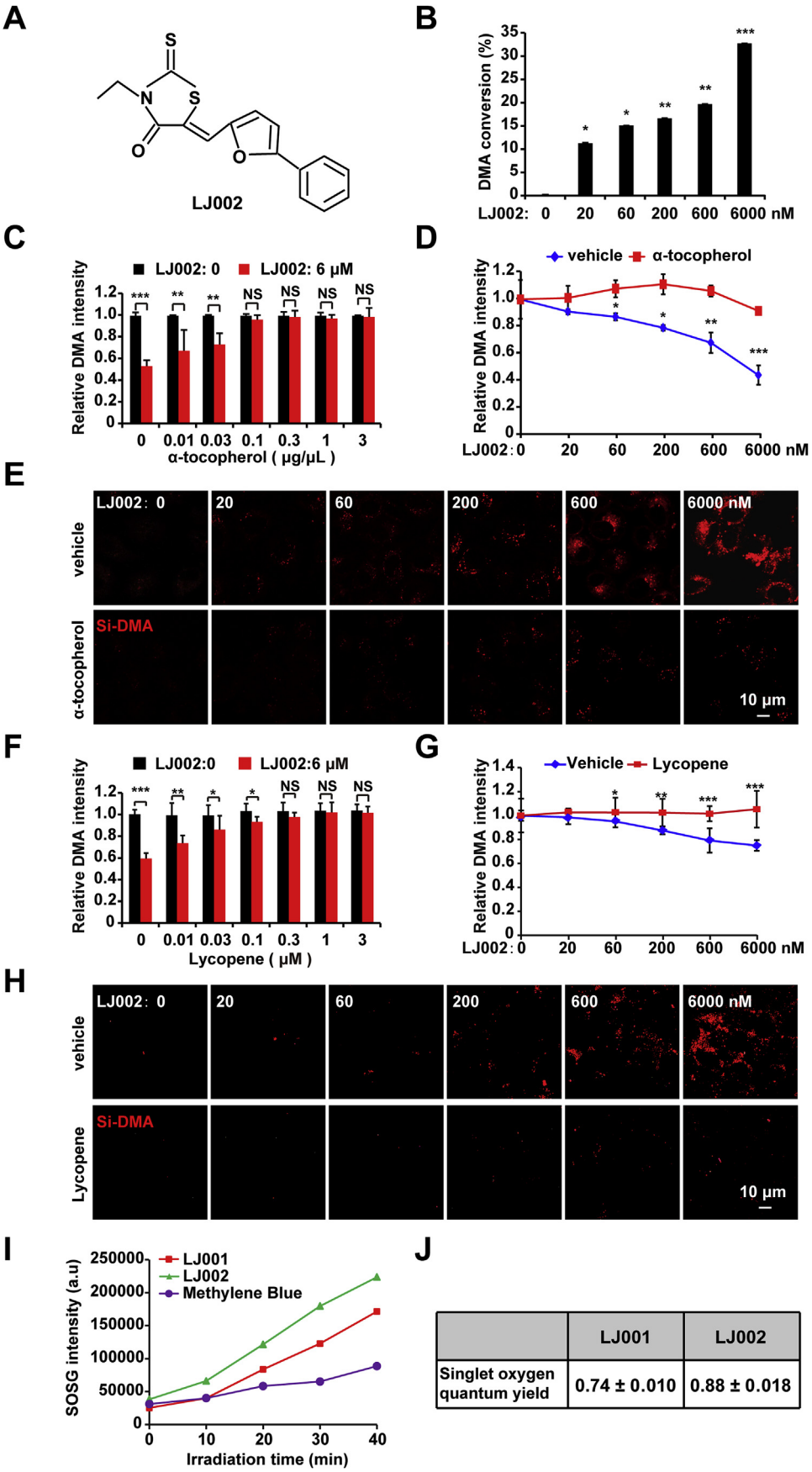

	LJ001	LJ002
Singlet oxygen quantum yield	0.74 ± 0.010	0.88 ± 0.018

Fig. 1. LJ002 generates $^1O_2$.

(A) Chemical structure of LJ002.

(B) Various concentrations of LJ002 were added to a solution of 0.5 μM DMA made with D_2O in the presence of light for 1 h at 25 °C. The disappearance of DMA's fluorescence signal was detected to estimate the generation of $^1O_2$. Data show the efficiency of DMA conversion.

(C) After 0.5 μM DMA was incubated with DMSO (LJ002: 0) or 6 μM LJ002 in the presence of α-tocopherol at various concentrations for 1 h, the fluorescence intensity of DMA was measured.

(D) The conversion of DMA by LJ002 was determined in the presence of 0 (vehicle) and 0.1 μg/μL α-tocopherol.

(E) PK-15 cells were incubated with 50 nM Si-DMA and different concentrations of LJ002. The generation of $^1O_2$ in the absence or presence of 0.1 μg/μL α-tocopherol for 1 h was observed under fluorescence microscopy.

(F) After 0.5 μM DMA was incubated with DMSO (LJ002: 0) or 6 μM LJ002 in the presence of lycopene at various concentrations for 1 h, the fluorescence intensity of DMA was measured.

(G) The conversion of DMA by LJ002 was determined in the presence of 0 (vehicle) and 1 μM lycopene.

(H) PK-15 cells were incubated with 50 nM Si-DMA and different concentrations of LJ002. The generation of $^1O_2$ in the absence or presence of 1 μM lycopene for 1 h was observed with fluorescence microscopy.

(I) After reaction of 1 μM SOSG with 6 μM LJ001, 6 μM LJ002 and 6 μM methylene blue for different irradiation times, the fluorescence intensity of SOSG was measured.

(J) Corresponding $^1O_2$ quantum yields for LJ001 and LJ002. The errors originate from the linear fit of the data. NS, not significant, *P < 0.05, **P < 0.01, ***P < 0.001, one-way ANOVA. (For interpretation of the references to color in this figure legend, the reader is referred to the Web version of this article.)

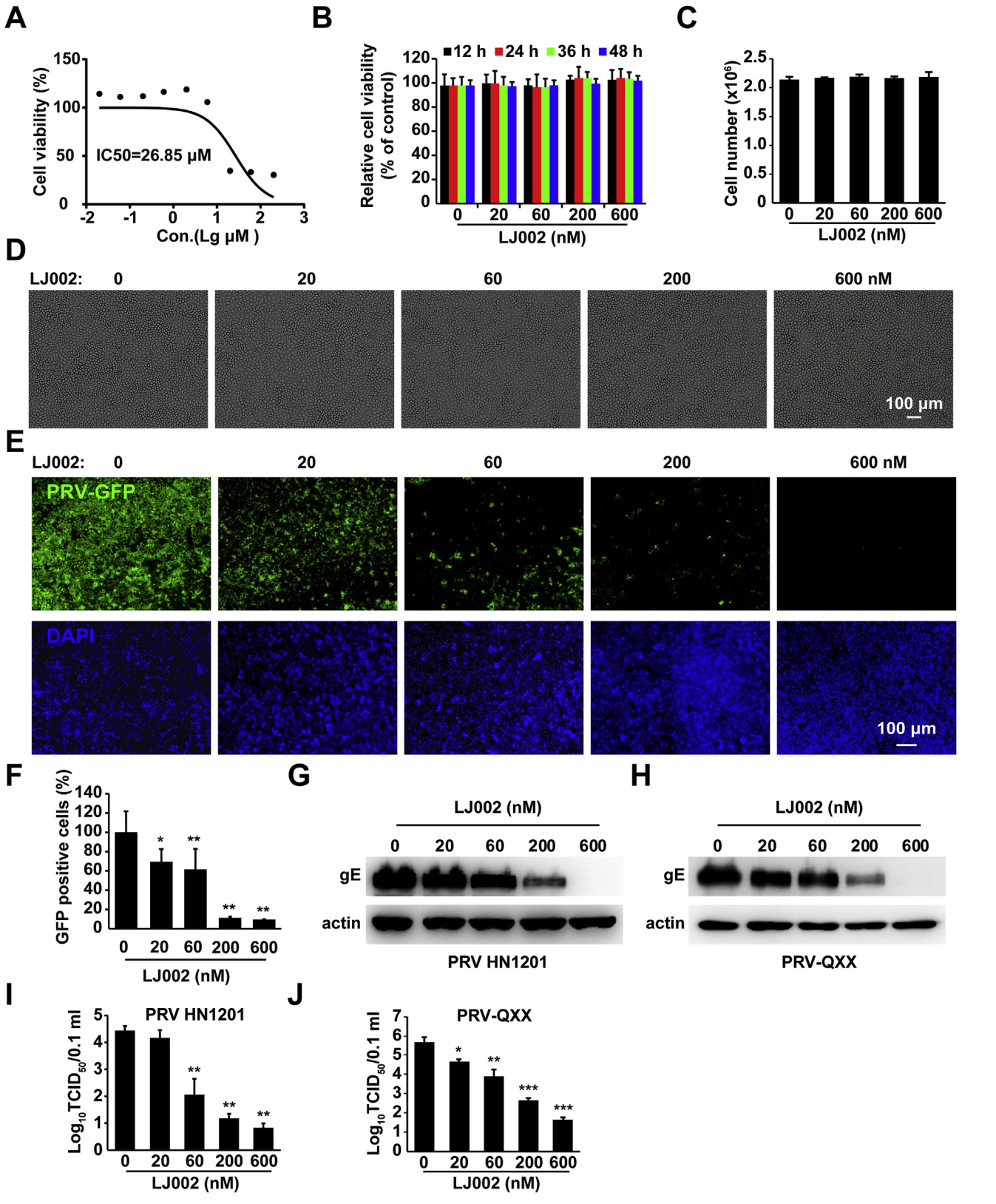

(caption on next page)

2.5. Flow cytometry

For viral proliferation assays, cells were infected with recombinant viruses expression the GFP reporter gene for 24–48 h and digested with trypsin-EDTA (25200072, GIBCO). Then, cells were collected by centrifugation and suspended in phosphate-buffered saline (PBS). The percentage of GFP positive cells was measured by flow cytometry on a BD AccuriC6 instrument. All data were analyzed in CytExpert software.

Fig. 2. LJ002 inhibits PRV replication.
(A) IC50 analysis of LJ002 in PK-15 cell lines. Cells were incubated with LJ002 at 0, 20 nM, 60 nM, 200 nM, 600 nM, 2 μM, 6 μM, 20 μM, and 60 μM doses. CCK assays were then used to determine the cell viability (%). IC50 values were determined after the absorbance values vs. various drug concentrations were plotted in GraphPad Prism. The graph was then fitted with a non-linear regression and sigmoid dose-response curve to obtain the IC50 values.
(B) Cell viability assays of PK-15 cells treated with LJ002 (0–600 nM) for 12, 24, 36, and 48 h.
(C and D) Cell number and representative bright-field microscopic images of PK-15 cells after treatment with DMSO (vehicle control) or LJ002 (20, 60, 200, and 600 nM) for 48 h. Fresh DMSO or LJ002 was added every 12 h.
(E) PK-15 cells were pretreated with various concentrations of LJ002 for 4 h and infected with PRV-GFP (MOI = 0.01) for 1 h at 37 °C, and then the infectious inoculum was replaced with growth medium containing LJ002 at the indicated concentrations for 36 h. Cells were fixed and stained with DAPI, and their fluorescence was detected with fluorescence microscopy.
(F) The GFP-positive PK-15 cells (with the same treatment as that in E) were measured by flow cytometry.
(G and H) Immunoblotting analysis of PK-15 cells treated as in E and infected with PRV HN1201 (MOI = 1, G) or PRV-QXX (MOI = 1, H) with the indicated antibodies.
(I and J) PK-15 cells treated as in E and infected with PRV HN1201 (MOI = 1, I) or PRV-QXX (MOI = 1, J). Viruses were harvested with three freeze-thaw cycles, and the viral titer was determined with $TCID_{50}$ assays. *P < 0.05, **P < 0.01, ***P < 0.001, one-way ANOVA.

2.6. Immunoblotting analysis

Whole cell lysates were prepared in RIPA buffer (50 mM Tris-HCl, pH 8.0, 150 mM NaCl, 1% Triton X-100, 1% sodium deoxycholate, 0.1% SDS, and 2 mM $MgCl_2$) supplemented with protease inhibitors (4693116001, Roche). The protein concentrations in the lysates were quantified with a Bicinchoninic Acid (BCA) Protein Assay Kit (BCA01, DINGGUO Biotechnology) and subjected to immunoblotting according to standard protocol. Immunoblotting results were visualized with Luminata Crescendo Western HRP Substrate (WBLUR0500, Millipore) on a GE AI600 imaging system.

2.7. Immunofluorescence

Cells grown on coverslips were fixed with 4% paraformaldehyde (PFA) for 30 min and incubated with PBS containing 10% FBS with the primary antibody (1:500) for 1 h at room temperature. After being washed three times with PBS, cells were labeled with fluorescent secondary antibody (1:500) for 1 h. Images were acquired with a Zeiss LSM800 confocal microscope and ZEN 2012 software. Images were quantified in ImageJ (National Institutes of Health) for quantitative image analysis.

2.8. RT-qPCR

Total RNA was isolated with Trizol Reagent and subjected to cDNA synthesis with an oligo (dT) or random hexamer primer. RT-qPCR was performed in triplicate with SYBR Premix Ex Taq according to the manufacturer's instructions, and data were normalized to the level of β-actin expression in each sample.

2.9. Viral titration and infectivity

The 50% tissue culture infective dose ($TCID_{50}$) assay was performed to assess viral titration and infectivity. On day 0, cells were seeded in 96-well plates at a density of 1×10^4 cells per well. On day 1, the cells were inoculated with serially ten-fold diluted viruses at 37 °C for 1 h. Excess viral inoculum was removed by washing with PBS. Then, 200 μL of maintenance medium (2% FBS/DMEM) was added to each well, and cells were cultured for another 3–5 days. Cells showing the expected cytopathic effects were counted daily, and the $TCID_{50}$ value was calculated with the Reed-Muench method.

Intracellular infectivity. Cells were washed three times with PBS, scraped, and pelleted by centrifugation at 1,000 g for 5 min. The cell pellets were subjected to three freeze-thaw cycles with liquid nitrogen and a thermal block set to 37 °C. Then, cell lysates were centrifuged at 10,000 g for 10 min at 4 °C to remove the cell debris. The titers of infectious viruses were expressed as $TCID_{50}$ per mL after a limiting dilution assay.

Extracellular infectivity. To determine the extracellular infectivity of the viruses, we harvested the supernatants, filtered them through a 0.45 μm pore size filter, and stored them at 4 °C. Their infectivity was determined in parallel with a limiting dilution assay, as described above.

2.10. EdU (5-ethynyl-2′-deoxyuridine) labeling and staining

For EdU labeling, Vero cells were cultured in 10% FBS/DMEM containing 25 μM EdU (C00052, RIBOBIO) and simultaneously infected with PRV HN1201 (MOI = 1) for 24 h. Viruses were harvested with three freeze-thaw cycles, and the viral titer was determined with $TCID_{50}$ assays.

For EdU staining, PK-15 cells were incubated with EdU-labeled PRV HN1201 (MOI = 15) and cell Mask™ Green at 4 °C for 1 h. Cells were then fixed in 4% PFA and stained with Apollo reaction cocktail (C00031*, RIBOBIO) at room temperature for 30 min. Images were captured on a Zeiss LSM 800 microscope and processed with ImageJ software for quantitative image analysis.

2.11. Measurement of $^1O_2$

In our experiments, LJ002 was added to solutions to achieve the proper final concentrations; the solutions were then irradiated with a light emitting diode (LED) (660 nm) for 60 min with a power density of 5 mW/cm^2 under a 1 atm oxygen atmosphere at room temperature.

The compound 9,10-dimethylanthracene (DMA) is a specific fluorescent $^1O_2$ trap, which reacts selectively with $^1O_2$ and forms the non-fluorescent 9,10-dimethylanthracene endoperoxide ($DMAO_2$). Thus, the disappearance of DMA's fluorescence signal was monitored and used to estimate the capacity of LJ002 to generate $^1O_2$. DMA fluorescence intensity was measured at excitation wavelength = 370 nm and emission wavelength = 432 nm with a microplate reader (Awareness Technology Inc.).

Si-DMA can selectively detect $^1O_2$: the fluorescence of Si-DMA increases 17 times as a result of endoperoxide formation at the anthracene moiety in the presence of $^1O_2$. In addition, Si-DMA can be used to visualize the real-time generation of $^1O_2$ from protoporphyrin IX in mitochondria with 5-aminolevulinic acid [36]. Cells were incubated with 50 nM Si-DMA and different concentrations of LJ002. The generation of $^1O_2$ was observed through fluorescence microscopy (640 nm irradiation).

2.12. Measurements of $^1O_2$ quantum yield of LJ002 by SOSG

Singlet Oxygen Sensor Green (SOSG) is a detection reagent that is highly selective to $^1O_2$. In the presence of $^1O_2$, SOSG reacts with $^1O_2$ and produces SOSG endoperoxides (SOSG-EP), which emit strong green fluorescence with a maximum at 531 nm [37]. Methylene blue (MB) is a phenothiazinium dye with a known singlet oxygen quantum yield of 0.52 [38]. After fixing the concentration of MB in aqueous solution, the

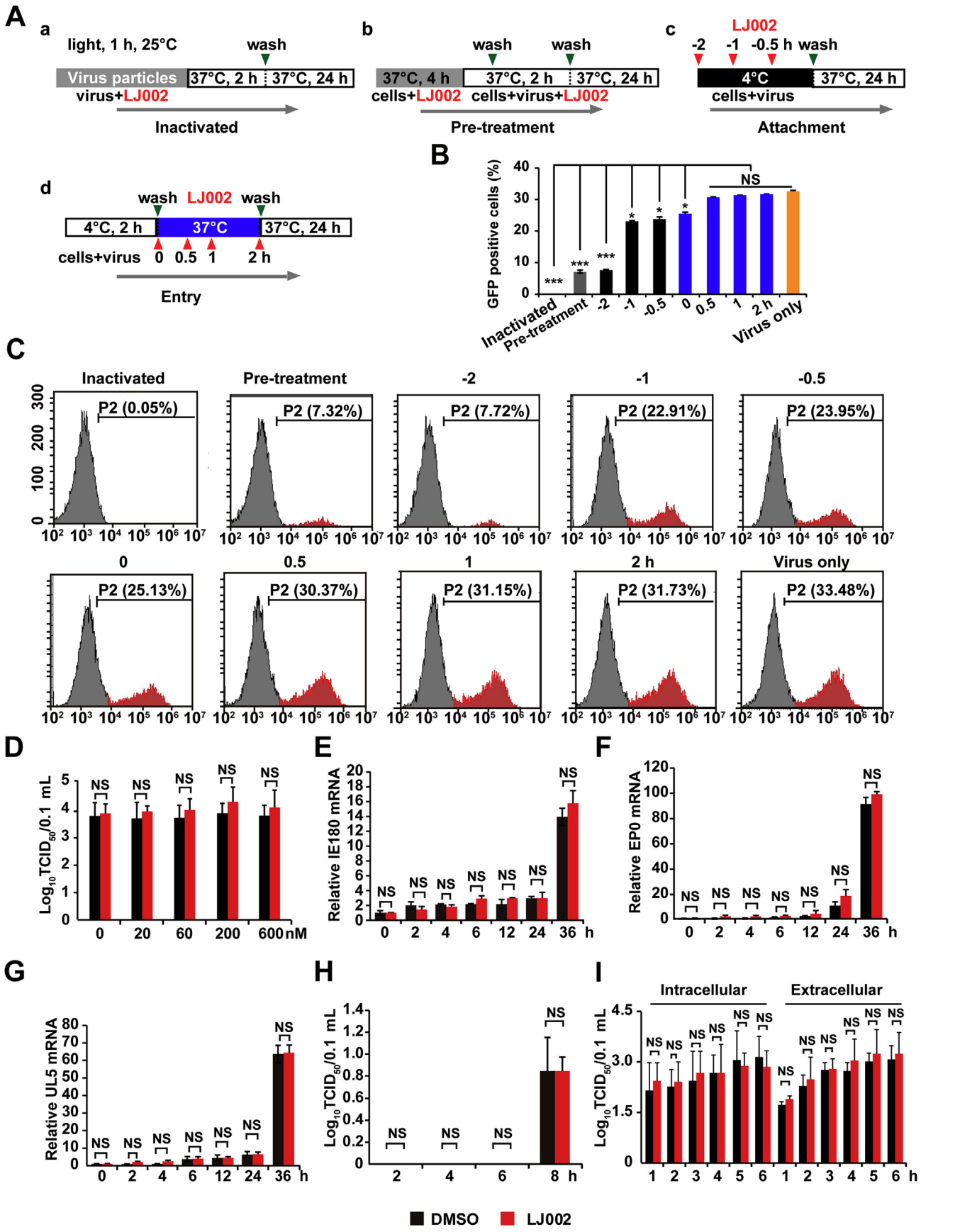

(caption on next page)

Fig. 3. Time-of-drug-addition analysis of LJ002's antiviral effect.
(A) Schematic of the effects of LJ002 treatment on PRV particles, viral attachment, and viral entry, with the indicated washing steps and incubation periods. For viral inactivation assays, PRV-GFP (MOI = 0.01) was pre-incubated with LJ002 in the presence of light for 1 h at 25 °C before inoculation of PK-15 cells. For pre-treatment assays, LJ002 was used for pretreatment of PK-15 cells at 37 °C for 4 h. For viral attachment assays, PK-15 cells were treated with LJ002 concurrently with PRV-GFP inoculum (MOI = 0.01) at 4 °C before washing and a temperature shift to 37 °C to facilitate entry of the virus. For viral entry assays, PRV-GFP-bound PK-15 cells (MOI = 0.01) were maintained at 4 °C and then treated with LJ002 at 37 °C before cells were washed. Virus only indicates normal virus infection without LJ002 treatment.
(B) The GFP-positive PK-15 cells after 24 h of incubation were measured by flow cytometry.
(C) Flow cytometry images of PRV-GFP proliferation in PK-15 cells treated as in B.
(D) PRV HN1201 (MOI = 0.1) viruses were used to infect PK-15 cells at 4 °C for 2 h; the temperature was shifted to 37 °C for 1 h (internalization), and the cells were washed with PBS and treated with various concentrations of LJ002 for 24 h. The viral titer was determined with $TCID_{50}$ assays.
(E–G) PK-15 cells were infected with PRV HN1201 (MOI = 0.1) at 4 °C for 2 h, shifted to 37 °C for 1 h (internalization), and then treated with DMSO or 600 nM LJ002 for 0–36 h. The mRNA levels of viral genes (IE180, E; EP0, F; UL5, G) were analyzed by RT-qPCR.
(H) PK-15 cells were infected with PRV HN1201 (MOI = 0.1) at 4 °C for 2 h, shifted to 37 °C for 1 h (internalization), and then treated with DMSO or 600 nM LJ002 for 2 h, 4 h, 6 h, or 8 h. The viral titer was determined with $TCID_{50}$ assays.
(I) PK-15 cells were infected with PRV HN1201 (MOI = 0.1) at 4 °C for 2 h, then shifted to 37 °C for 12 h. After 12 h, the cells were replaced with DMSO or 600 nM LJ002 for 1–6 h. The supernatants and intracellular viral fluids were collected at different time points, and the viral titers were determined. NS, not significant, *P < 0.05, ***P < 0.001, one-way ANOVA.

reaction rate (r) of SOSG with $^1O_2$ can be obtained by using time dependent SOSG fluorescence enhancement data, which are proportional to the concentration of SOSG-EP:

$$r = \frac{d[SOSG-EP]}{dt} = k[SOSG]^n[^1O_2]$$

[SOSG-EP] is the concentration of SOSG-EP; [SOSG] and [$^1O_2$] are the concentrations of SOSG and $^1O_2$, respectively; and n is the order of reaction with respect to SOSG. When n = zero, r is dependent on only [$^1O_2$]. In this case, we define the reaction of SOSG with $^1O_2$ as an "n-zero reaction". As a result, the concentration of $^1O_2$ generated by photosensitization of MB can be quantitatively determined from the reaction rate (r).

To determine the minimal concentration of SOSG to meet the n-zero reaction condition, various concentrations of SOSG were used to react with $^1O_2$ generated by 1 μM MB photoirradiation in PBS. Furthermore, measurements were performed to explore the feasibility of quantitative measurement of $^1O_2$ generation from the photosensitization of various MB concentrations by keeping the SOSG concentration constant. As demonstrated in previous studies, the reaction rate of the $^1O_2$ fluorescence probes' oxidation by $^1O_2$ can be determined from the initial region of the kinetic curve, thus allowing for quantification of $^1O_2$ generation [39]. Therefore, as an additional test, we estimated the $^1O_2$ quantum yield of LJ002 by comparing the reaction rate of a known photosensitizer by using SOSG after photosensitization. In this study, the $^1O_2$ quantum yield of LJ002 was determined with respect to MB as a standard photosensitizer as follows [40]:

$$\Phi_{\Delta LJ002} = \frac{r_{LJ002}/A_{LJ002}}{r_{MB}/A_{MB}} \cdot \Phi_{\Delta MB}$$

where r_{LJ002} and r_{MB} are the reaction rates of the SOSG with $^1O_2$ generated from photosensitization of LJ002 and MB, respectively. A_{LJ002} and A_{MB} are the absorbance of LJ002 and MB, respectively, and $\Phi_{\Delta MB}$ (0.52) is the $^1O_2$ quantum yield of MB.

2.13. Determination of lipid oxidation

For lipid oxidation assays, we used a commercial kit to quantify the generation of MDA according to the manufacturer's protocol for the Lipid Peroxidation MDA Assay Kit (20130407, Nanjing, China). In brief, after treatment, cell lysates were extracted in 250 μL of RIPA buffer with a syringe needle and centrifuged at 12,000 g for 5 min at 4 °C. The supernatant was subjected to MDA measurement with a spectrophotometer (excitation at 379 nm and emission at 432 nm). The MDA values were normalized to the total cellular protein content, which was determined with a BCA Protein Assay Kit.

2.14. Liquid chromatography-mass spectrometry (LC-MS) analysis of MDA

LC-MS experiments were carried out on a Xevo TQ-S (Waters). PRV (1.05×10^9 $TCID_{50}$) was exposed to different concentrations of LJ002 for 1 h at room temperature and broken by ultrasonic crushing. For preparation of samples, an aliquot of 250 μL sample (viral homogenate) was placed in a 1.5 mL microcentrifuge tube, and 50 μL of 6 M NaOH was added. Alkaline hydrolysis of protein bound MDA was achieved by incubation of this mixture in a 60 °C water bath for 40 min. Then, protein was precipitated with 125 μL of 35% (v/v) perchloric acid and mixed with 25 μL of DNPH, prepared as a 5 mM solution in 2 M hydrochloric acid. Finally, this reaction mixture was incubated for 30 min at room temperature, protected from light. The derived samples were centrifuged at 20,000 rpm for 10 min, filtered with a 0.22 μm filter membrane, and used as samples in MS determination (ion source: EI+; scanning mode: SRM; capillary voltage: 2.00 KV; cone pore voltage: 29.0 V; ion source temperature: 150 °C; desolvent gas temperature: 500 °C; desolvent airflow velocity: 1000 L/Hr).

2.15. Transmission electron microscopy (TEM)

PK-15 cells were incubated with PRV HN1201 (MOI = 10, pretreated with DMSO or LJ002) at 4 °C for 2 h, washed with PBS, fixed for 30 min at room temperature with 2.5% glutaraldehyde, embedded and processed for TEM.

To image the viral morphology by negative staining, we incubated purified PRV HN1201 with LJ002 in the presence of light for 1 h and fixed samples with glutaraldehyde in phosphate buffer to a final concentration of 0.5% at 4 °C for 30 min. Then 5 μL of PRV suspension was adsorbed to glow-discharged electron microscopy grids and stained with 2% phosphotungstic acid. The grids were desiccated and visualized by TEM.

2.16. Atomic force microscopy (AFM)

AFM analysis was conducted with an MFP3D Infinity-Asylum Research AFM in tapping mode (Oxford Instruments PLC). Briefly, PRV HN1201 (final viral titer of 2×10^8 $TCID_{50}$/mL) was incubated with LJ002 in the presence of light for 1 h and pipetted onto a freshly cleaved mica surface, which was air-dried in a dust-free enclosure before use. Imaging was performed with uncoated silicon cantilevers AC160TS-R3 from Oxford Instruments PLC, with a tip radius of 7 nm, resonance frequency of approximately 200–300 kHz, and spring constant of 8.4–57 k (N/m). Images with a scan size of 1×1 μm^2/4.5×4.5 μm^2/20×20 μm^2 and resolution 512×512 pixels^2 were obtained with scan rates between 0.6 and 1.0 Hz and set points close to 0.2 V. AFM images were analyzed offline in AFM software (Microsoft).

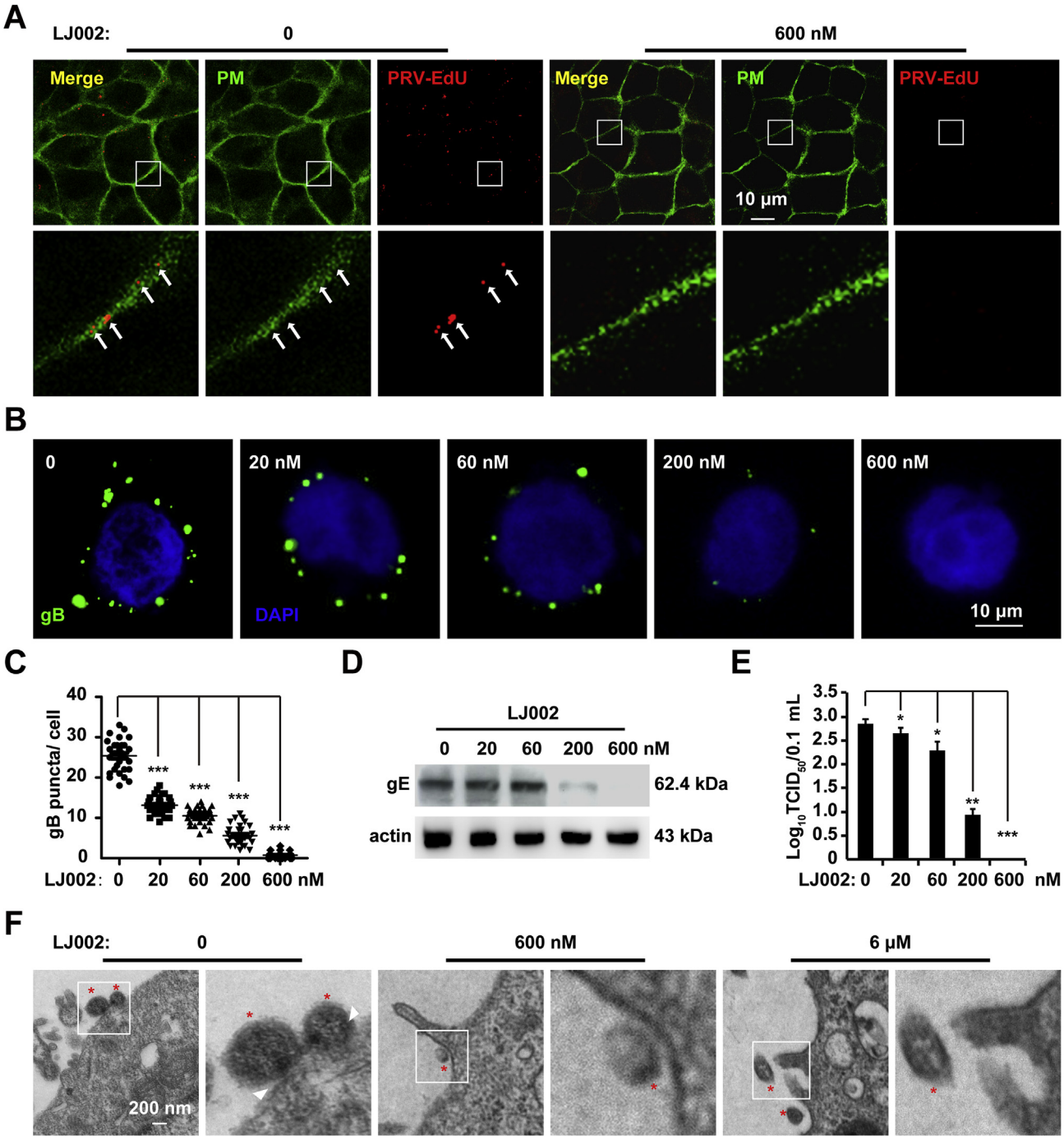

Fig. 4. LJ002 treatment inactivates PRV and impairs viral attachment/fusion to host cells.

(A) PRV HN1201 (MOI = 1, labeled with EdU) was treated with DMSO or LJ002 (600 nM) in the presence of light for 1 h at 25 °C and then washed with PBS and subjected to repurification by centrifugation through an ultrafiltration spin-column. The viruses were used to infect PK-15 cells at 4 °C for 2 h, and the cells were then stained with Apollo (PRV) and CellMask™ Green (PM). The labeled viruses (red) attached/fused with membranes of the host cells were analyzed by confocal microscopy.

(B) PRV HN1201 (MOI = 10) was treated with various concentrations of LJ002 in the presence of light for 1 h at 25 °C and then washed with PBS and subjected to repurification by centrifugation through an ultrafiltration spin-column. The repurified viruses were used to infect PK-15 cells at 4 °C for 2 h, and the cells were washed with PBS and fixed with 4% PFA. The viral glycoprotein (gB) on PK-15 cells was stained with *anti*-gB, and the nuclei were stained with DAPI. The fluorescence of gB was analyzed by confocal microscopy.

(C) The number of gB puncta per cell was counted in 30 cells per group.

(D) The repurified viruses (MOI = 10) as in Fig. 4B were used to infect PK-15 cells at 4 °C for 2 h; the cells were then washed with PBS, and the viral envelope glycoprotein (gE) on PK-15 cells was analyzed by immunoblotting.

(E) The repurified viruses (MOI = 1) as in Fig. 4B were used to infect PK-15 cells, and the viral titer was determined with $TCID_{50}$ assays.

(F) The repurified viruses (MOI = 10) as in Fig. 4B were used to infect PK-15 cells at 4 °C for 2 h; the cells were washed with PBS, fixed, and processed for TEM. Red asterisks indicate the virus particles; white arrowheads show the attachment/fusion of viruses with cell membranes. *P < 0.05, **P < 0.01, ***P < 0.001, one-way ANOVA. (For interpretation of the references to color in this figure legend, the reader is referred to the Web version of this article.)

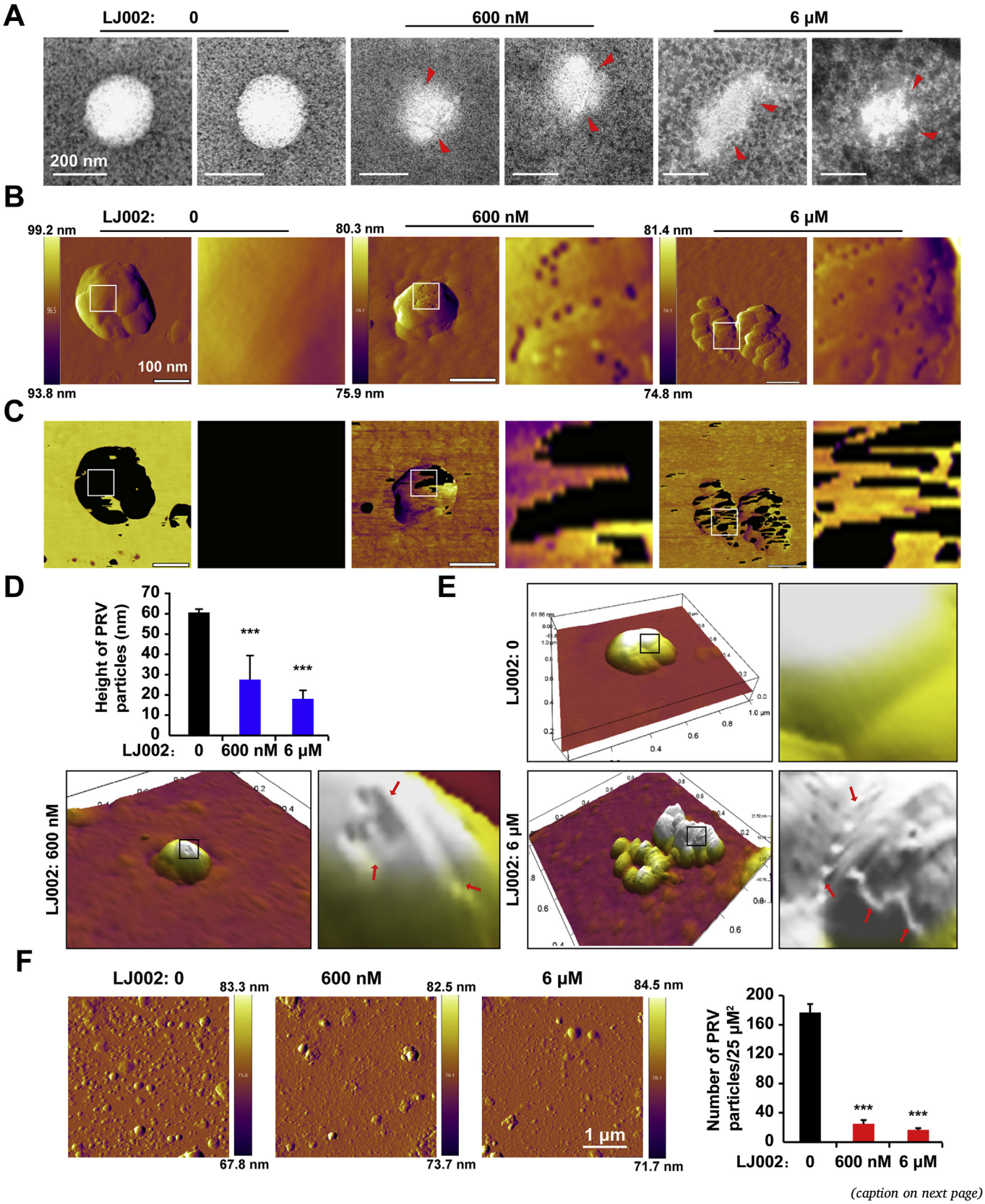

(caption on next page)

2.17. Histological analysis

Tissues dissected from mice were fixed in 4% PFA overnight, embedded in paraffin, and sectioned for hematoxylin and eosin (H&E) staining. To determine the expression of PRV gB in brain sections, we used immunofluorescence. Briefly, brain sections were stained with *anti*-gB (1:200), then incubated with secondary antibody (anti-mouse IgG antibody labeled with Alexa Fluor 488, 1:200) and labeled with DAPI. All sections were photographed at a magnification of 400 × .

Fig. 5. LJ002 induces substantial distortion of the viral membrane.
(A) Purified and concentrated PRV HN1201 was treated with DMSO (0), 600 nM or 6 μM LJ002, and incubated at 25 °C for 1 h; the cells were a fixed with 0.5% glutaraldehyde at 4 °C for 30 min, stained with 2% phosphotungstic acid, and visualized with negative-stain electron microscopy. Arrowheads indicate disrupted parts of the PRV particles.
(B and C) AFM deflection images (B) and phase images (C) of the PRV HN1201 treated with DMSO (0), 600 nM or 6 μM LJ002, and incubated at 25 °C for 1 h. Insets in B and C show high-resolution images recorded in the square regions.
(D) Cross-sectional analysis reveals the height profile of PRV treated with LJ002.
(E) 3D AFM image of PRV treated with LJ002. Insets show high-resolution images recorded in the square regions. Red arrows indicate the minor ditches and uneven edges caused by LJ002 treatment.
(F) Purified and concentrated PRV HN1201 was treated with DMSO (0), 600 nM or 6 μM LJ002, and incubated at 25 °C for 1 h; the amounts of viral particles adsorbed per unit surface of mica were measured with AFM. ***$P < 0.001$, one-way ANOVA. (For interpretation of the references to color in this figure legend, the reader is referred to the Web version of this article.)

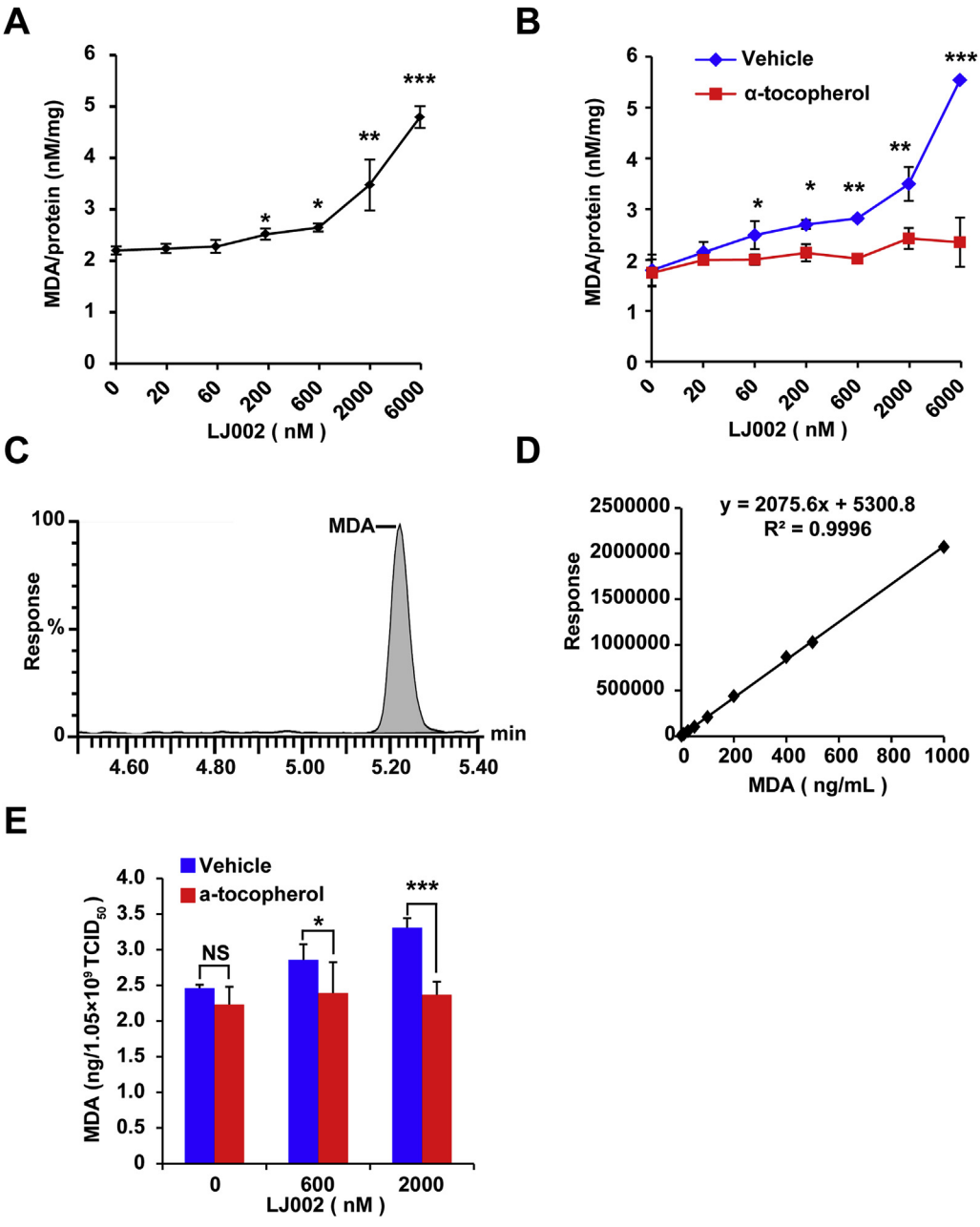

Fig. 6. LJ002 treatment increases the generation of the lipid oxidation product MDA.
(A) PK-15 cells were treated with DMSO or various concentrations of LJ002, and exposed to light for 1 h. The concentrations of MDA were determined with MDA assay kits and normalized to the cellular protein content.
(B) PK-15 cells were incubated with different concentrations of LJ002, and the generation of MDA in the absence or presence of 0.1 μg/μL α-tocopherol for 1 h was determined as in Fig. 6A.
(C) Chromatogram of standard MDA analyzed by LC-MS.
(D) Calibration plot for MDA at increasing concentrations.
(E) The PRV (1.05×10^9 $TCID_{50}$) and different concentrations of LJ002 were exposed to light for 1 h at room temperature. Then, the levels of MDA were determined by LC-MS. NS, not significant, *$P < 0.05$, **$P < 0.01$, ***$P < 0.001$, one-way ANOVA.

2.18. PRV purification by iodixanol density gradient centrifugation

PRV in the supernatant was purified by ultracentrifugation through Optiprep iodixanol density gradients. Briefly, 200 mL PRV supernatant was transferred into a dialysis bag, and PEG12000 was added to concentrate the culture fluid to a final concentration of 10% (v/v). After centrifugation at 20,000 rpm for 2 h at 4 °C, the viral precipitate was suspended in 1 mL PBS (pH 7.2) and loaded with 7.2 mL of 20% iodixanol solution (v/v). The viral separation was performed by ultracentrifugation for 2 h at 30,000 rpm at 4 °C. The fractions were

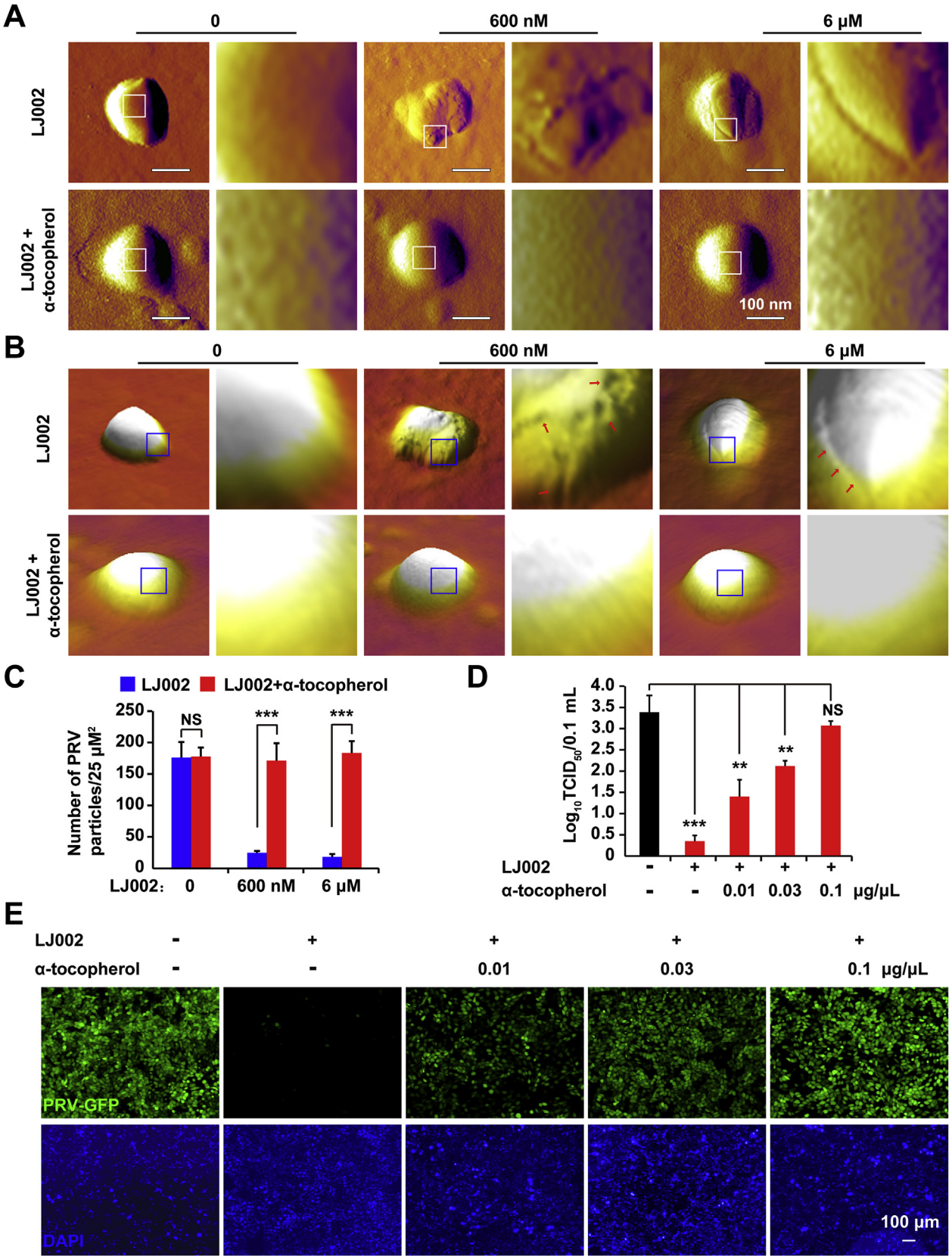

(caption on next page)

Fig. 7. α-tocopherol abrogates viral envelope damage and restores the LJ002-mediated decrease in viral infectivity.
(A and B) AFM deflection images (A) and 3D AFM images (B) of LJ002-treated PRV-1201 without or with simultaneous addition of α-tocopherol (0.1 μg/μL). Insets show high-resolution images recorded in the square regions.
(C) LJ002 was added to PRV HN1201 without or with α-tocopherol (0.1 μg/μL) and exposed to light for 1 h; the amount of viral particles adsorbed per unit surface of mica was measured with AFM.
(D) LJ002 was added to PRV HN1201 (MOI = 0.1) without or with various concentrations of α-tocopherol and exposed to light for 1 h; then the virus was used to infect PK-15 cells for 24 h. The viral titer was determined with $TCID_{50}$ assays.
(E) LJ002 was added to PRV-GFP (MOI = 1) without or with various concentrations of α-tocopherol and exposed to light for 1 h; then the virus was used to infect PK-15 cells for 36 h. Cells were fixed and stained with DAPI, and their fluorescence was detected with fluorescence microscopy. NS, not significant, **P < 0.01, ***P < 0.001, one-way ANOVA.

collected, and $TCID_{50}$ and dot blotting analyses were used to determine the infectivity and the presence of PRV structural glycoproteins.

2.19. LC-MS/MS analysis

To verify the changes in PRV proteins in response to singlet oxygen challenge, we exposed purified PRV particles to vehicle or 600 nM LJ002 for 1 h (660 nm, 5 mW/cm^2), then performed capillary liquid chromatography/tandem mass spectrometry (LC-MS/MS) by using an EASY-nLC1200 system (Thermo Fisher Scientific) coupled to a Q-Exactive mass spectrometer (Thermo Fisher Scientific), which was operated in positive ion mode (LumingBio, Shanghai). Samples were loaded on a C18 nanoLC trap column (100 μm × 20 mm, C18) and washed with nano-HPLC buffer A (0.1% formic acid). A gradient of 5–35% nano-HPLC buffer B acetonitrile (60% ACN, 0.1% formic acid) was used to elute the sample on a C18 column (75 μm × 150 mm), both at a flow rate of 300 nl/min. A data-dependent acquisition MS method was used, in which one full scan (300–1600 m/z, R = 60,000 at 200 m/z) at a target of 1×10^6 ions was first performed, followed by ten data-dependent MS/MS scans with higher-energy collisional dissociation.

2.20. Dot blot assay

Reaction of the circulating antibodies to PRV was evaluated with dot blotting, in which 2.5 μL purified PRV was dotted on a nitrocellulose membrane and blocked with 10% FBS for 1 h at room temperature. These viral dots were then incubated with different dilutions (1:1, 1:2, 1:4, 1:8, 1:16, 1:32, 1:64, 1:128, 1:256, and 1:512) of serum collected from mice immunized with PRV (formalin) or PRV (LJ002). The membrane was subjected to immunoblotting according to standard protocol.

2.21. Serum neutralization assays

The neutralizing activity of serum specimens against PRV was determined with an in vitro neutralization assay. First, sera were incubated at 56 °C for 30 min to inactivate complement. Then, two-fold serial dilutions of sera were mixed with equal volumes of 200 $TCID_{50}$ of PRV HN1201 and incubated at 37 °C for 1 h. The mixtures were added in triplicate to wells of a 96-well plate containing PK-15 cells. PRV-specific cytopathic effects were observed, and neutralization titers were calculated as the $\log_2$ of the reciprocal of the highest dilution resulting in complete neutralization.

2.22. Mouse experiments

Female 6–8-week-old Kunming mice were purchased from the Center of Experimental Animal of Zhengzhou University (Zhengzhou, China) and maintained in a specific-pathogen-free animal facility according to the Guide for the Care and Use of Laboratory Animals and the related ethical regulations at Henan Agricultural University. Sacrifice was performed with isoflurane narcosis followed by cervical dislocation in accordance with the rules approved by the State Council of the People's Republic of China for experimental animal care and use.

Eight mice per group were subcutaneously (S.C.) inoculated with conventional formalin or LJ002-inactivated PRV HN1201 vaccine. The clinical signs of the mice were monitored daily, and survival as a Kaplan-Meier plot was compared with the log-rank (Mantel-Cox) test in GraphPad Prism (GraphPad Software, Inc.)

To determine the protective effect of LJ002 inactivated PRV in mice, we injected two groups of mice were injected S.C. with conventional formalin or LJ002-inactivated PRV HN1201 for immunization, and booster vaccination was performed 28 days later. The mice were challenged S.C. with PRV (2×10^6 $TCID_{50}$, death dose) at 28 days after the first or second immunization. Clinical signs were recorded daily for up to 21 days.

2.23. Hemagglutination (HA) assays

Viruses from infected cells were harvested with three freeze-thaw cycles. The samples were then serially diluted with PBS in V-bottom 96-well plates and incubated with 0.5% of chicken red blood cells at 37 °C for 15 min. The viral HA titer was the highest dilution at which agglutination was observed.

2.24. Statistical analysis

Data were obtained from at least three independent experiments for quantitative analyses and are expressed as means ± standard errors of the means. All statistical analyses were performed with one-way analysis of variance (ANOVA). Significant differences relative to the corresponding controls were accepted at $^*P < 0.05$, $^{**}P < 0.01$, and $^{***}P < 0.001$.

3. Results

3.1. LJ002 generates $^1O_2$ in solution and living cells

To evaluate the capacity of LJ002 (Fig. 1A) for generating $^1O_2$, we added LJ002 to DMA, a well-known chemical trap for $^1O_2$, which selectively reacts with $^1O_2$ and forms the non-fluorescent 9,10-endoperoxide [28]. In D_2O solution, LJ002 exhibited dose-dependent $^1O_2$-mediated oxidation of DMA (Fig. 1B). Addition of an antioxidant (α-tocopherol [41], a scavenger of $^1O_2$) abrogated LJ002-induced DMA oxidation (Fig. 1C and D). We also used Si-DMA [36] to detect the generation of $^1O_2$ in living cells, as shown in Fig. 1E. With increasing LJ002 concentrations, the fluorescence intensities of Si-DMA were also enhanced. However, the simultaneous addition of α-tocopherol to cells abolished the fluorescence enhancement of Si-DMA mediated by $^1O_2$. Furthermore, we found that lycopene, the most efficient biological carotenoid $^1O_2$ quencher [42], also had a significant quenching effect on $^1O_2$ produced by LJ002 (Fig. 1F–H). Fig. 1I demonstrated that the SOSG-EP fluorescence intensity of LJ002 was higher than those of LJ001 and MB. Moreover, the $^1O_2$ quantum yield of LJ002 was quantitatively determined to be approximately 0.88 ± 0.018 by comparison of the reaction rate of SOSG that reacted with MB (Fig. 1J). Thus, LJ002 produces $^1O_2$ both in solution and in living cells.

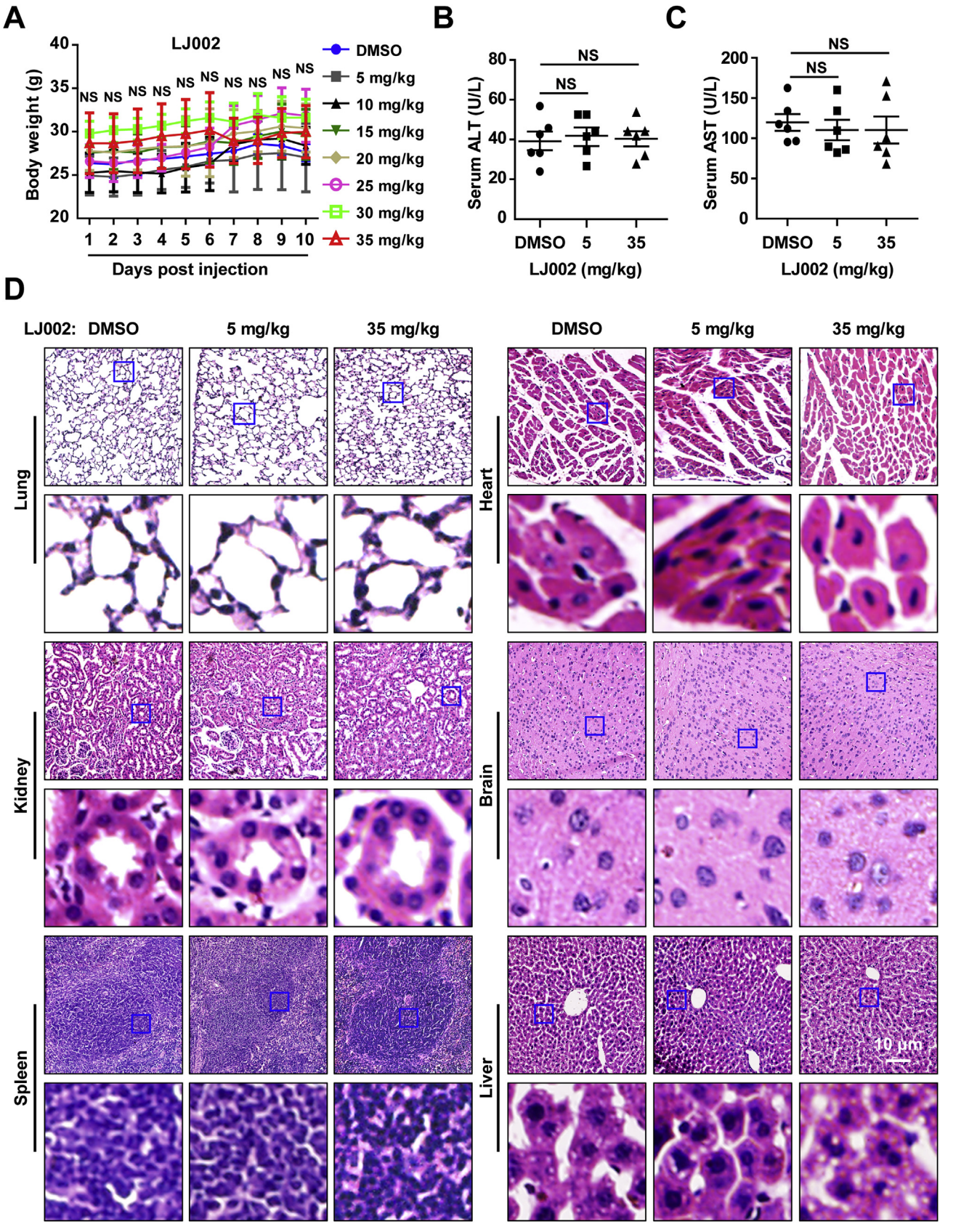

(caption on next page)

Fig. 8. LJ002 exhibits no clear *in vivo* toxicity.
(A) Female 8-week-old mice (n = 5 per group) were injected S.C. daily for 10 days with 100 μL DMSO or LJ002 at 5 (low), 10, 15, 20, 25, 30, and 35 (high) mg/kg doses. Daily averaged weights of the mice in each group are shown.
(B and C) On day 10, terminal blood samples were collected via cardiac puncture, and the activity of serum ALT and AST was measured. Results shown are averages for six individual animals.
(D) Representative micrographs of H&E-stained sections. Tissues were harvested from mice treated with DMSO, 5 mg/kg or 35 mg/kg of LJ002 daily for 10 days. NS, not significant, one-way ANOVA.

3.2. LJ002 inhibits PRV replication in vitro

To examine a possible application of LJ002 in the control of viral diseases in animal husbandry, we used PRV as a model to study swine enveloped virus diseases and their inhibition. We first determined the effect of LJ002 on cell proliferation. The IC50 value for LJ002 was 26.85 μM, on the basis of the cell viability/proliferation rates in PK-15 cells measured with CCK-8 assays (Fig. 2A). Cell viability assays (Fig. 2B) and cell number counting (Fig. 2C) showed that treatment with 0–600 nM of LJ002 for 12–48 h was not harmful to PK-15 cells. Microscopically, there were no changes in cellular morphology when fresh DMSO or LJ002 was added every 12 h for as many as 2 days (Fig. 2D). Then, we tested whether LJ002 inhibited PRV at low (sub-micromolar) concentrations. PK-15 cells were pretreated with LJ002 (600 nM) for 4 h and infected with PRV-GFP, PRV HN1201, and PRV-QXX. For all these viruses, LJ002 was effective at inhibiting PRV infection in a dose-dependent manner, as determined by fluorescence microscopy (Fig. 2E), flow cytometry (Fig. 2F), immunoblotting (Fig. 2G and H), and $TCID_{50}$ (Fig. 2I and J) assays. These data demonstrate that LJ002 treatment inhibits PRV infection.

3.3. LJ002 prohibits viral early entry-related steps

To further characterize the molecular mechanism of LJ002's antiviral activity, we performed a time-of-drug-addition assay wherein the drug was directly added to free virus particles (Fig. 3A, a. Inactivated), added to cells 4 h before PRV-GFP infection (Fig. 3A and b. Pre-treatment), or added to viral inoculum at 4 °C on the PK-15 cell monolayer (Fig. 3A, c. Attachment). At this temperature, viral particles can bind to the cell surface, but subsequent fusion/entry steps are precluded until the temperature is shifted to 37 °C [43]. In addition, we concurrently added the drug at the time of viral infection (Fig. 3A, d. Entry) and incubated cells for 24 h before measuring the GFP positive cells by flow cytometry. Time-of-addition experiments (Fig. 3A–C) indicated that LJ002 inhibited PRV infectivity when it was added before or during the early entry events of infection. Moreover, LJ002's *anti*-PRV activity appeared strongest when the viral particles were pre-incubated with LJ002 in the presence of light for 1 h, and nearly 100% inhibition was achieved, thus suggesting that LJ002 can directly inactivate these free virus particles and neutralize their infectivity.

We next determined the antiviral activity of LJ002 in controlling the spread of established infections. PRV particles were allowed to first bind the PK-15 cell surface at 4 °C before the temperature was shifted to 37 °C for 1 h to allow viral entry. The inocula were then removed, and cells were incubated with or without the compound. As shown in Fig. 3D, LJ002 was ineffective in limiting the growth of PRV. Furthermore, mRNA expression results also indicated that addition of LJ002 after viral entry did not affect the transcription of the immediate-early 180 gene (Fig. 3E; IE180), early gene (Fig. 3F; EP0), and DNA replication-related gene (Fig. 3G; UL5). As observed in the viral replication and release assays, there was no significant inhibition of viral replication (Fig. 3H) and release (Fig. 3I) when LJ002 was added in the post-infection phase. Together, these data provide evidence that LJ002 inactivates PRV virions and impairs early entry-related processes, thus suppressing viral infection.

3.4. LJ002 inhibits viral attachment/fusion to host cells

To further demonstrate that LJ002 acts on the virus, we pretreated live PRV particles with LJ002, washed and repurified the virions from excess compound, and examined the infectivity of the repurified PRV particles. When cells were infected with PRV containing EdU labeled viral genome and Apollo stained, in the control group, EdU-labeled viruses were mainly detected on the plasma membrane, whereas the PRV viruses inactivated by LJ002 were nearly undetectable (Fig. 4A). As shown by the immunofluorescence signals of gB, PRV particles were attached to the surfaces of PK-15 cells, and the exposure to LJ002 resulted in a dose-dependent inhibition of PRV virion attachment to cells (Fig. 4B and C). Similar results were obtained from the detection of PRV envelope gE content on cells in immunoblotting assays (Fig. 4D). As shown in Fig. 4E, approximately 100% of infectivity was lost when PRV was pretreated with 600 nM LJ002. Further support for these findings was provided by electron micrographs showing that PRV virions attached and partially fused with the plasma membrane in the control group, whereas viruses inactivated by LJ002 were noninfectious and did not attach/fuse on the cell surface. In addition, the viral particles also showed some distortions in the viral membrane (Fig. 4F).

3.5. LJ002 causes viral membrane deformation

Because viral membrane distortions were observed when cells were infected with LJ002-inactivated PRV particles (Fig. 4F), we sought to determine whether the virion morphology might become deformed after LJ002 treatment. We first examined untreated and treated virions by negative-stain electron microscopy. As shown in Fig. 5A, the viral envelope of untreated PRV virons was intact, whereas exposure to LJ002 led to disruption of the envelope and distortion of viral ultrastructure. The surfaces of viruses exposed to 600 nM LJ002 appeared rougher, and their shapes appeared less regular. The distortions in the membrane were more pronounced after 6 μM LJ002 treatment. The presence of negative staining inside virions treated with LJ002, but not untreated virions, suggested permeabilization of the viral membrane. To further confirm that LJ002 compromises viral membrane integrity, we used AFM to assess the morphological changes induced in membrane structure and organization. The AFM deflection images of PRV, as shown in Fig. 5B, were taken after the viruses were treated with DMSO (the vehicle control) or LJ002. The surfaces of PRV particles without treatment were very smooth, whereas those treated with LJ002 were much rougher and showed some peculiar topographic features. AFM phase imaging has been used to detect surface information, such as different surface chemical compositions, adhesion, flexibility, and other properties, and the different phases show different shades of color (or shading) [44]. The untreated virions mainly showed one phase, thus indicating that they were single-component particles. In response to increasing concentrations of LJ002, the phase images clearly showed two distinct phases, thereby indicating that the viral surface composition had changed (Fig. 5C). The heights of untreated virions were significantly greater than those of LJ002-treated virions (Fig. 5D). Higher magnification, and a three-dimensional (3D) view revealed that exposure to LJ002 disrupted the envelope and caused indentations (arrows) in the viral units (Fig. 5E). Differences in the values of particle adsorption on mica are associated with hydrophobic interactions between the particles and the surfaces [45]. The number of PRV particles

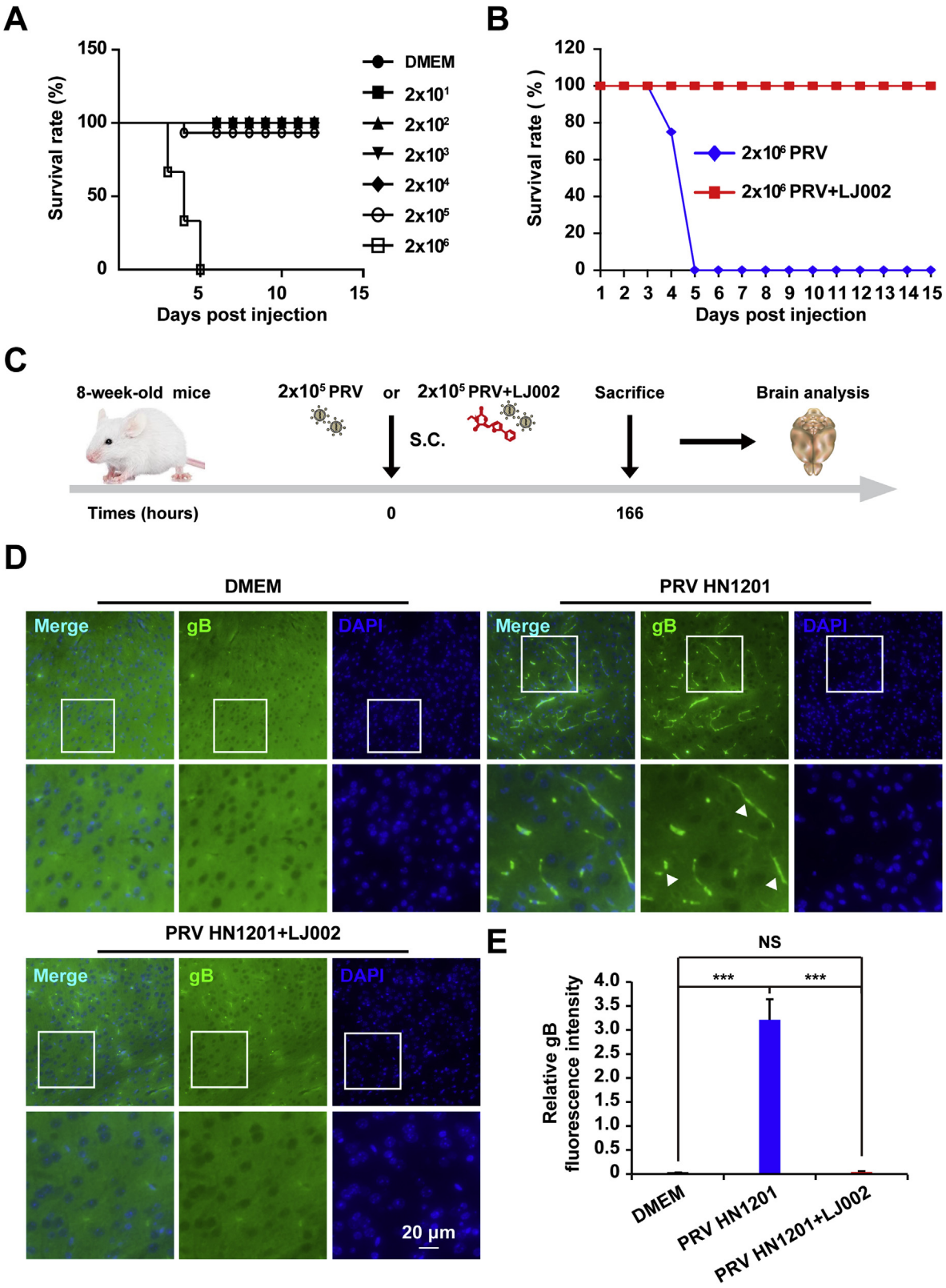

Fig. 9. LJ002 protects mice against life-threatening PRV infection.

(A) 8 week old mice (n = 10 per group) were S.C. infected with PRV HN1201 at doses ranging from 2×10^1 to 2×10^6 $TCID_{50}$, and the survival rate was monitored.

(B) 8 week old mice (n = 10 per group) were injected with 2×10^6 $TCID_{50}$ of PRV HN1201 (DMEM) or LJ002-inactivated PRV HN1201 (LJ002), and the survival rate was recorded daily.

(C) Experimental strategy for S.C. infection of PRV HN1201 (2×10^5 $TCID_{50}$) or LJ002-inactivated PRV HN1201 (2×10^5 $TCID_{50}$).

(D) Mice infected with PRV as in C were euthanized after 166 h, sections of brains were prepared, and immunofluorescence analysis was conducted with *anti*-gB. The boxed region is enlarged below. The arrowhead indicates PRV positive infection in the brain cortex.

(E) The relative fluorescence intensity of gB was analyzed in Image J and normalized to the number of nuclei. NS, not significant, ***P $<$ 0.001, one-way ANOVA.

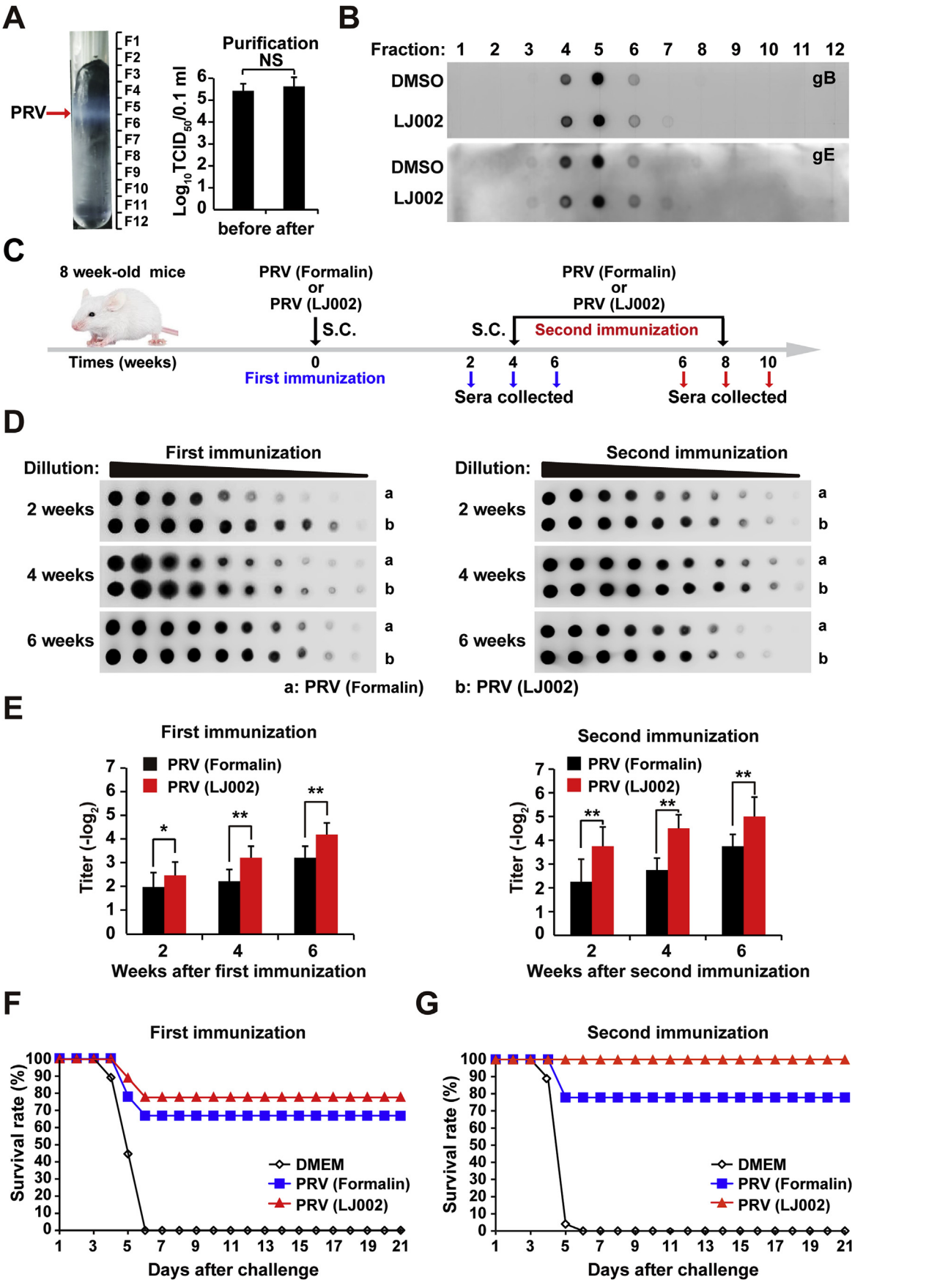

(caption on next page)

Fig. 10. Mice immunized with LJ002-inactivated PRV show more efficient protection than mice immunized with conventional formalin-inactivated PRV vaccine.
(A) The arrow indicates the band of concentrated PRV particles after iodixanol density gradient centrifugation. This PRV HN1201-containing band was collected for subsequent $TCID_{50}$ analysis.
(B) PRV particles were pretreated with DMSO or LJ002 in the presence of light for 1 h, and then purified by iodixanol density gradient centrifugation. The content of glycoproteins (gB and gE) on the virus was detected by dot blotting.
(C) Experimental strategy for S.C. injection of conventional formalin or LJ002-inactivated PRV HN1201 (2×10^6 $TCID_{50}$) at 0 (first immunization) and 4 (second immunization) weeks. Anti-sera were collected at various time points after the first immunization and the second immunization.
(D) Each group of mice (n = 8) was immunized (S.C.) with formalin or LJ002 inactivated PRV as shown in C. Serum samples were collected at various time points, and the circulating antibodies reacting to PRV were determined by dot blot ELISA.
(E) Each group of mice (n = 8) was immunized (S.C.) with formalin or LJ002 inactivated PRV as shown in C. Serum samples were collected at various time points, and the PRV-specific neutralizing antibodies were determined by serum neutralization assays.
(F) Each group of mice (n = 8) was immunized S.C. with DMEM, formalin, or LJ002 inactivated PRV for 4 weeks; after the first immunization, mice were challenged with 2×10^6 $TCID_{50}$ of PRV HN1201 (lethal dose). The survival rate was monitored daily for 21 days after challenge.
(G) Each group of mice (n = 8) was immunized S.C. with DMEM, formalin, or LJ002 inactivated PRV for 4 weeks; the booster was administered with the same quantities of inactivated virus. At 4 weeks after secondary immunization, mice were challenged with 2×10^6 $TCID_{50}$ of PRV HN1201 (lethal dose). The survival rate was monitored daily for 21 days after challenge. $^*P < 0.05$, $^{**}P < 0.01$, one-way ANOVA.

adsorbed on mica whose surface was treated with the aforementioned compound was significantly lower than that in the control group, thus suggesting that the hydrophobicity of the viral surface had changed (Fig. 5F).

3.6. LJ002 increases the production of MDA

PRV is an enveloped virus surrounded by a lipid membrane derived from host cell membranes. Because LJ002 induced a substantial distortion in the viral membrane, we hypothesized that LJ002 might generate $^1O_2$ within the plane of the viral membrane, and $^1O_2$-mediated lipid oxidation might result in damage to the architecture of the viral membrane, thus hindering virus-cell membrane fusion. To determine whether $^1O_2$ contributes to oxidative degradation of lipids, we examined the generation of MDA, a well-known secondary product of lipid oxidation [46]. As shown in Fig. 6A, MDA levels significantly increased in LJ002-treated cells in a dose-dependent manner, as compared with the levels in the control group. In contrast, the content of MDA did not increase after the administration of α-tocopherol (Fig. 6B). To explore whether LJ002 directly affected the lipid composition of viral membranes, we treated purified PRV particles with LJ002 and analyzed the viral MDA content by LC-MS, owing to its high analytical sensitivity and specificity [47]. A typical chromatogram for the MDA standard is shown in Fig. 6C. Standard calibration graphs were prepared for various MDA concentrations, and a typical fitting line is shown in Fig. 6D. The high-resolution LC-MS spectral analysis revealed that LJ002-treated viruses had significantly more oxidized lipids than LJ002-treated viruses supplemented with α-tocopherol (Fig. 6E), thus indicating the specific and direct oxidation of lipids in viral membranes by LJ002-induced $^1O_2$.

3.7. α-tocopherol abrogates LJ002-induced viral envelope destruction

Because administration of the antioxidant resulted in $^1O_2$ clearance and decreased lipid oxidation, we next investigated the effects of α-tocopherol on LJ002-induced viral membrane deformation and the antiviral activity of LJ002. By comparing the AFM topography images obtained in the absence and presence of α-tocopherol after 1 h of incubation with LJ002, we observed that the lipid envelope of LJ002 treated PRV was considerably damaged, but these membrane deformations were reverted by the addition of α-tocopherol, after which a smooth viral surface comparable to that in the DMSO group was observed (Fig. 7A and B). Moreover, α-tocopherol administration significantly attenuated the LJ002-induced reduction of PRV particles adsorbed on mica, thereby supporting the notion that lipid oxidative injury contributes to changes in the hydrophobicity of the viral surface (Fig. 7C). With increased concentrations of α-tocopherol, both the viral titer (Fig. 7D) and PRV-GFP fluorescence assay results (Fig. 7E) showed that the addition of the $^1O_2$ scavenger reversed the antiviral activity of LJ002 against PRV. Together, our results confirm the specific involvement of $^1O_2$ in LJ002's destruction of the viral envelope and its antiviral activity.

3.8. LJ002 does not produce adverse side effects

The potential toxicity of LJ002 was next assessed systematically. Growth of mice was not affected by treatment with LJ002 in any of the doses assayed, on the basis of body weight (Fig. 8A) and external appearance. None of the recipient mice died from exposure to these LJ002 doses. Liver damage or hepatotoxicity in recipient mice was analyzed by measurements of serum alanine aminotransferase (ALT) and aspartate aminotransferase (AST) levels. As shown in Fig. 8B and C, the normal serum ALT and AST levels following treatment indicated no significant liver damage caused by 5 mg/kg or 35 mg/kg per day of LJ002 treatment for 10 consecutive days. Moreover, in a macroscopic analysis, none of the mice showed histomorphologic changes resulting from LJ002 treatment. The toxicity to major organs was also investigated with H&E staining. No appreciable abnormalities or noticeable organ damage was apparent in any of the organs analyzed, regardless of experimental group (Fig. 8D). These results provide direct evidence that the prepared LJ002 has negligible tissue toxicity.

3.9. LJ002 protects mice against life-threatening PRV infection

We next investigated the potential antiviral activity of LJ002 against PRV *in vivo*. To define the virulence of PRV HN1201, we performed S.C. inoculation of 8-week-old mice with viral doses ranging from 2×10^1 to 2×10^6 $TCID_{50}$. Infection with 2×10^6 $TCID_{50}$ PRV HN1201 induced 100% mortality by day 5 post injection; thus, the infection progressed rapidly. Infection with 2×10^5 $TCID_{50}$ resulted in a survival rate of 90% (Fig. 9A). In mice lethally challenged with 2×10^6 $TCID_{50}$ of PRV HN1201, we observed high mortality, and all mice died within 5 days post infection. In comparison, mice infected with LJ002-inactivated PRV HN1201 showed 100% survival rate in 15 days observation (Fig. 9B). Because PRV tends to infect neurons in the central nervous system, we also examined viral proliferation in the brain tissue of the infected mice (schematic outline in Fig. 9C). Using an immunofluorescence staining method, we found that the brain tissues of mice infected with PRV exhibited positive viral antigen gB signals, whereas the DMEM (mock infection) group and the group receiving LJ002-inactivated PRV showed negative viral signals (Fig. 9D and E). Our results demonstrated that PRV infection can be inhibited *in vivo* by pre-incubation with LJ002.

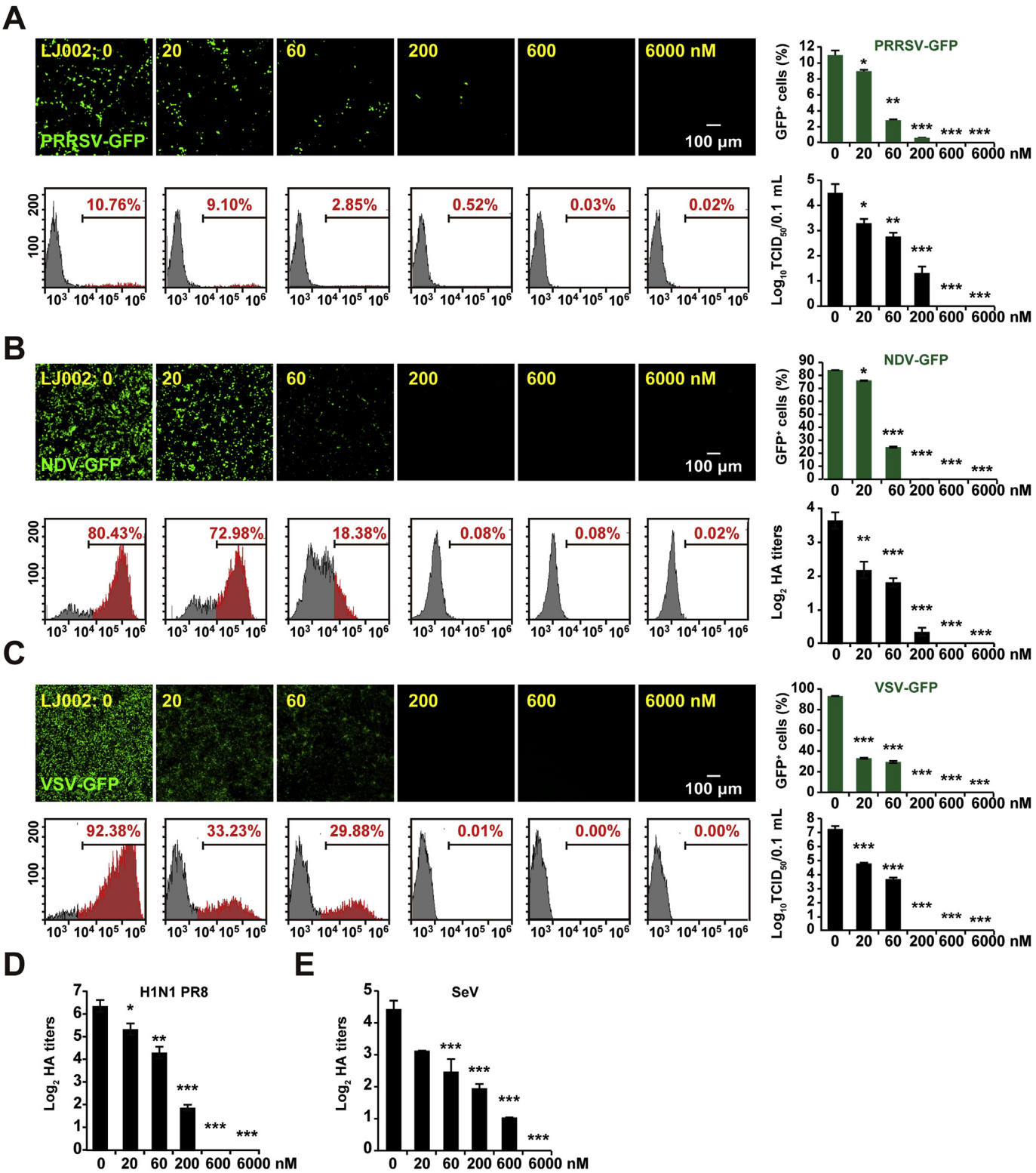

Fig. 11. LJ002 exhibits broad antiviral activity against enveloped viruses.

(A) MARC-145 cells were infected with various concentrations of LJ002-inactivated PRRSV-GFP virus (MOI = 10) for 48 h, and the viral replication was determined with fluorescence, flow cytometry, and $TCID_{50}$ assays. Gray peaks: GFP-negative cells (cells not infected with PRRSV); red peaks: GFP-positive cells (cells infected with PRRSV).

(B) PK-15 cells were infected with various concentrations of LJ002-inactivated NDV-GFP (MOI = 0.001) for 12 h, and viral replication was determined with fluorescence and flow cytometry assays. The titer of NDV-GFP was tested with HA assays.

(C) Vero cells were infected with various concentrations of LJ002-inactivated VSV-GFP virus (MOI = 0.001) for 48 h, and viral replication was determined with fluorescence, flow cytometry, and $TCID_{50}$ assays.

(D) HeLa cells were infected with various concentrations of LJ002-inactivated H1N1-PR8 (MOI = 1) for 12 h, and the titer of H1N1-PR8 was tested with HA assays.

(E) PK-15 cells were infected with various concentrations of LJ002-inactivated SeV (MOI = 1) for 12 h, and the titer of SeV was tested with HA assays. *P < 0.05, **P < 0.01, ***P < 0.001, one-way ANOVA. (For interpretation of the references to color in this figure legend, the reader is referred to the Web version of this

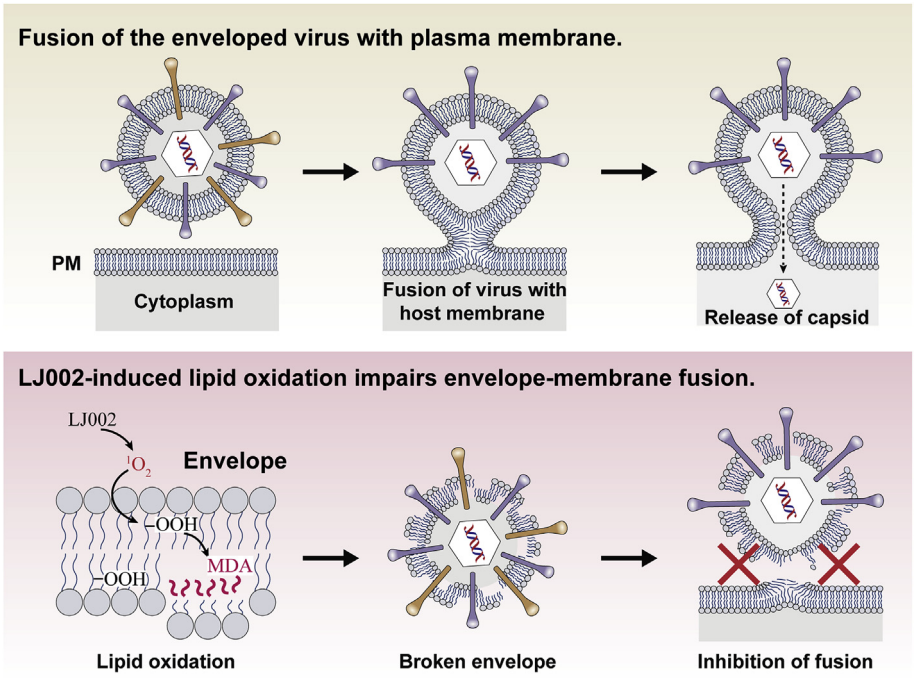

Fig. 12. $^1O_2$ generated by LJ002 oxidizes lipids in the viral envelope, thus impairing viral envelope-cell membrane fusion and inhibiting viral entry into cells.

3.10. LJ002-inactivated PRV confers more efficient protection than conventional inactivated PRV vaccine

On the basis of our data on *in vivo* LJ002-inactivated PRV, we explored the potential applications of LJ002 and its ability to generate PRV vaccines. Viral antigen content after LJ002 inactivation provides an indicator of surface protein alterations after viral inactivation treatment. First, we optimized the method of iodixanol density gradient ultracentrifugation to purify PRV and verified that the purification process did not affect the titer of the virus (Fig. 10A). We used this method to analyze essential proteins such as viral antigen gB or primary virulence factor gE. As shown in Fig. 10B, the content of gB and gE on the virus was not affected. Nevertheless, the LC-MS/MS spectrum showed that the oxidative modification of viral polypeptides increased after LJ002 treatment (Fig. S1). To further investigate the immunity generated by vaccination with LJ002 or conventional formalin-inactivated PRV vaccine, we collected and analyzed anti-sera (schematic outline in Fig. 10C). We investigated circulating antibodies induced by vaccination by using a dot blot assay. This assay is a sensitive and specific technique to measure circulating antibody responses to the same content of PRV on the dot. Serum samples were collected at various time points and analyzed with a two-fold serial dilution. As shown in Fig. 10D, sera from mice that received LJ002-inactivated vaccination showed significantly higher circulating antibody titers than sera from conventional formalin-inactivated PRV mice. Serum samples were further evaluated for their ability to neutralize PRV in vitro in serum neutralization assays. As shown in Fig. 10E, detectable neutralizing antibodies were developed in the sera of mice immunized with either PRV (formalin) or PRV (LJ002). However, after either a single or booster immunization, the highest levels of neutralizing antibodies were observed in the sera of mice immunized with PRV (LJ002), results similar to the dot-blot antibody responses. These experimental results indicate that vaccination with LJ002-inactivated virus induces better neutralizing antibody immune responses.

To evaluate the potency of the LJ002-inactivated vaccine against lethal PRV challenge, we immunized mice as described and subjected them to challenge with a 100% lethal dose of PRV HN1201 delivered S.C. at 4 weeks after first or secondary immunization. The survival rates are shown in Fig. 10F and G. Mice that received formalin or LJ002 inactivated PRV demonstrated significant protection when challenged with a lethal dose of PRV. Single or multiple exposures to this LJ002-inactivated vaccine led to better protection than that in mice receiving conventional formalin-inactivated vaccine. All mice in the control group (immunized with DMEM) died from the challenge. In summary, these results indicate that the LJ002 is significantly more efficient than the conventional formalin agent in vaccine preparation.

3.11. LJ002 is a broad antiviral

Our studies showed that LJ002-mediated $^1O_2$ oxidizes the viral membrane, thereby blocking the fusion of viral-cell membranes and exerting antiviral activity. We sought to examine the breadth of this inhibition by using phylogenetically distinct viruses. PRRSV (*Arteriviridae*), NDV (*Paramyxoviridae*), VSV (*Rhabdoviridae*), Sendai virus (*Respirovirus*), and Avian influenza virus (H1N1, *Orthomyxoviridae*) were inactivated with LJ002, and the viral replication was evaluated by fluorescence, flow cytometry, $TCID_{50}$, and HA assays. Despite the different viruses, target cell types, and assay readouts measuring infectivity, when treated with 600 nM LJ002, PRRSV, NDV, and VSV showed undetectable GFP-expression and $TCID_{50}$ (Fig. 11A–C). The HA titer also showed that 600 nM LJ002 pre-treatment inhibited H1N1 influenza virus replication (Fig. 11D). SeV exhibited a similar destructive efficiency with 600 nM of LJ002, and when LJ002 was increased to 6000 nM in the treatment, SeV was completely inactivated according to the HA titer data (Fig. 11E). Collectively, these results demonstrated that LJ002 has a broad-spectrum effect on viruses with lipid membranes.

4. Discussion

In mammals, enzymes such as myeloperoxidase have long been known to form $^1O_2$ [48]. $^1O_2$ has recently been shown to be essential for neutrophil extracellular trap formation and to regulate blood pressure under inflammatory conditions [24]. Chemical photosensitized reactions are a simple and controllable method for the production of $^1O_2$, requiring only oxygen and light of an appropriate wavelength. A group

of photosensitizers exemplified by LJ001, JL118, and JL122 are $^1O_2$ generators that exhibit antiviral activity in vitro. Unfortunately, the injection of these compounds has not been found to protect mice against lethal emerging pathogens, given the lack of light inside animal bodies [27,28]. In our study, we evaluated the novel $^1O_2$-generating agent LJ002, as an alternative to the classic inactivant for inactivated virus vaccine preparation. We found that LJ002 was able to produce $^1O_2$, both in solution and in living cells, which was quenched by antioxidants (Fig. 1). Cellular toxicity assays revealed that the cytotoxicity to cells was as high as 26.85 μM (IC50), possibly because of the cells' powerful free radical scavenging system. At the concentration of 600 nm, there was no effect on cell viability, number, and morphology, but proliferation of PRV was significantly inhibited (Fig. 2).

PRV is a member of the *Alphaherpesvirinae* subfamily, which primarily infects swine and has numerous other hosts, including rodents, ruminants, and carnivores, and causes nearly 100% mortality [49]. Some European countries and New Zealand have eradicated Pseudorabies via immunization with gE-deleted vaccines (particularly Bartha-K61) [50]. However, the pig industry in China has suffered considerable economic losses because of the reemergence of PRV variant strains since 2011 [5]. More seriously, previous reports have described PRV infections in three immunocompetent humans [51]. One case of human endophthalmitis has been confirmed to be caused by PRV after direct contact with contaminants [4]. In addition, our experiments demonstrate that PRV can infect human cell lines. This evidence indicates that PRV might infect humans, thus underscoring the necessity of mandatory PRV vaccination of swine and workers in the swine breeding industry. Therefore, we used PRV as a model to evaluate the antiviral effect of LJ002 and its potential use in animal husbandry.

Time-of-addition results revealed that LJ002 targets PRV's early entry steps, specifically inactivating cell-free virions and impeding viral attachment/fusion to the surface of host cells, thus abolishing subsequent infection (Figs. 3 and 4). By comparing the nanoscopic scale AFM topography images obtained before and after incubation with LJ002, we tracked the viral surface phase, height, and morphological changes, as well as the decreased hydrophobicity in LJ002-treated virions (Fig. 5). Phospholipids are a main component of biological membranes, and unsaturated phospholipids have C=C double bonds, which are highly vulnerable to lipid oxidation attack [52]. The clustering of oxidized phospholipids results in differential lipid packing, increased positive curvature, decreased membrane thickness and fluidity, and changes in the nanoarchitecture of the membrane that are not conducive to fusion [53]. In the present study, we demonstrated that LJ002 treatment caused a marked increase in the content of MDA on both cells and purified PRV particles (Fig. 6). Importantly, with antioxidant treatment, the generation of lipid oxidation products was decreased, the viral envelope was protected from damage, and viral infectivity was restored (Figs. 6 and 7). Because LJ002 caused no substantial morphological changes in cells, we speculate that its effects may be due to viral membranes derived from host cells lacking these metabolic and repair pathways, thus leaving their static membranes susceptible to LJ002 treatment.

Along with the high effectiveness of viral inactivation by LJ002, no signs of adverse side effects were observed in the body weights, serum biochemical markers, and histological examinations of the treated mice (Fig. 8). The actual efficacy of LJ002 in the prophylactic and immune protection of enveloped viral diseases is likely to depend on viral inactivation as well as on the pathogenic profile of the virus. Therefore, we conducted preliminary LJ002-mediated PRV inactivation efficacy experiments *in vivo* through lethal challenge of mice immunized with PRV or LJ002-inactivated PRV at the same $TCID_{50}$. Encouragingly, LJ002 did show efficacy: compared with the control group, the LJ002 treated group showed a 100% survival rate, and no viral protein expression was observed in the mouse brain (Fig. 9).

Antigen content and stabilized antigen structure are crucial for efficient presentation of antigenic peptides on the major histocompatibility complex, thus triggering effective immune responses [54]. Lipid oxidation may directly damage the transmembrane counterpart of membrane proteins or cause structural changes due to envelope disintegration. PRV gB and gE are envelope glycoproteins that are major viral antigens and participate in the processes of viral entry into host cells [55]. To assess the antigenic degradation during inactivation, we monitored the antigenic mass by dot blotting and clearly verified that lipid oxidation cannot affect the antigenic mass throughout the LJ002 inactivation processes. More encouragingly, our mouse data showed that LJ002-inactiviated PRV vaccine had distinct advantages over conventional formalin-inactivated vaccine in terms of humoral immune responses and protective efficacy (Fig. 10). Although $^1O_2$ produced by LJ002 can cause an increase in the oxidative modification of PRV proteins (Fig. S1), it does not affect the content of PRV proteins, nor does it affect the production of circulating/neutralizing antibodies. In addition, LJ002 inactivates a broad spectrum of viruses with lipid membranes (Fig. 11).

According to our work, we speculate that LJ002-mediated $^1O_2$ may be useful in inactivating ASFV. ASFV is a large, enveloped, double-stranded DNA virus with five layers: the genome-containing nucleoid (the first layer) is surrounded by a thick protein layer (the second layer), which is wrapped with a lipid-bi-layer membrane (the third layer) and an icosahedral protein capsid (the fourth layer); ASFV then buds through the plasma membrane and gains an external envelope (the fifth layer) [9]. Recently, results have indicated that inactivated ASFV does not confer protection, even in the presence of various adjuvants, thus suggesting that antibodies induced by ASFV structural protein might not be sufficient to protect pigs against virulent ASFV challenge [56]. Our results demonstrated that LJ002-mediated $^1O_2$ can oxidize lipids and destroy the membrane structure (Fig. 12). Therefore, epitopes that are not easily exposed and proteins that can elicit effective neutralizing antibodies or cell-mediated immune responses may be exposed.

Considering all these factors, we believe that the LJ002-inactivated vaccine has promise to be developed as a safe and efficacious vaccine against viral disease. Further studies are needed to obtain large amounts of statistical data to draw affirmative conclusions regarding the use of LJ002-inactivated vaccine for PRV protection, for ASFV protection in natural host systems, and for protection against other important pathogens such as severe acute respiratory syndrome-related coronavirus and Ebola virus.

Declaration of competing interest

The authors declare no conflicts of interest.

Acknowledgments

This work was supported by grants from the Ten Thousand Talents Program for Young Talents of China (W03070106), Outstanding Talents of Henan Agricultural University (30600773), the Training Plan of Young Key Teachers in Colleges and Universities of Henan Province (2016GGJS-033), Natural Science Foundation of Henan Province (83), National Natural Science Foundation of China (31802165).

Appendix A. Supplementary data

Supplementary data to this article can be found online at https://doi.org/10.1016/j.redox.2020.101601.

References

[1] A. Dehove, J. Commault, M. Petitclerc, M. Teissier, J. Mace, Economic analysis and costing of animal health: a literature review of methods and importance, Rev. Sci. Tech. 31 (605–17) (2012) 591–604.
[2] P. Daszak, A.A. Cunningham, A.D. Hyatt, Anthropogenic environmental change and

the emergence of infectious diseases in wildlife, Acta Trop. 78 (2001) 103–116.
[3] S. Verpoest, B. Cay, H. Favoreel, N. De Regge, Age-dependent differences in pseudorabies virus neuropathogenesis and associated cytokine expression, J. Virol. 91 (2017).
[4] J.W. Ai, S.S. Weng, Q. Cheng, P. Cui, Y.J. Li, H.L. Wu, Y.M. Zhu, B. Xu, W.H. Zhang, Human endophthalmitis caused by pseudorabies virus infection, China, 2017, Emerg. Infect. Dis. 24 (2018) 1087–1090.
[5] T.Q. An, J.M. Peng, Z.J. Tian, H.Y. Zhao, N. Li, Y.M. Liu, J.Z. Chen, C.L. Leng, Y. Sun, D. Chang, G.Z. Tong, Pseudorabies virus variant in Bartha-K61-vaccinated pigs, China, 2012, Emerg. Infect. Dis. 19 (2013) 1749–1755.
[6] J. Arzt, W.R. White, B.V. Thomsen, C.C. Brown, Agricultural diseases on the move early in the third millennium, Vet. Pathol. 47 (2010) 15–27.
[7] A. Gogin, V. Gerasimov, A. Malogolovkin, D. Kolbasov, African swine fever in the North Caucasus region and the Russian Federation in years 2007-2012, Virus Res. 173 (2013) 198–203.
[8] X. Zhou, N. Li, Y. Luo, Y. Liu, F. Miao, T. Chen, S. Zhang, P. Cao, X. Li, K. Tian, H.J. Qiu, R. Hu, Emergence of african swine fever in China, 2018, Transbound Emerg. Dis. 65 (2018) 1482–1484.
[9] N. Wang, D. Zhao, J. Wang, Y. Zhang, M. Wang, Y. Gao, F. Li, J. Wang, Z. Bu, Z. Rao, X. Wang, Architecture of African swine fever virus and implications for viral assembly, Science (2019), https://doi.org/10.1126/science.aaz1439.
[10] A.A. Aguirre, Changing patterns of emerging zoonotic diseases in wildlife, domestic animals, and humans linked to biodiversity loss and globalization, ILAR J. 58 (2017) 315–318.
[11] P.P. Pastoret, P. Jones, Veterinary vaccines for animal and public health, Dev. Biol. 119 (2004) 15–29.
[12] N. Bardiya, J.H. Bae, Influenza vaccines: recent advances in production technologies, Appl. Microbiol. Biotechnol. 67 (2005) 299–305.
[13] A. Moghaddam, W. Olszewska, B. Wang, J.S. Tregoning, R. Helson, Q.J. Sattentau, P.J. Openshaw, A potential molecular mechanism for hypersensitivity caused by formalin-inactivated vaccines, Nat. Med. 12 (2006) 905–907.
[14] N.K. Blackburn, T.G. Besselaar, A study of the effect of chemical inactivants on the epitopes of Rift Valley fever virus glycoproteins using monoclonal antibodies, J. Virol. Methods 33 (1991) 367–374.
[15] J.A. Swenberg, B.C. Moeller, K. Lu, J.E. Rager, R.C. Fry, T.B. Starr, Formaldehyde carcinogenicity research: 30 years and counting for mode of action, epidemiology, and cancer risk assessment, Toxicol. Pathol. 41 (2013) 181–189.
[16] H.G. Bahnemann, Inactivation of viral antigens for vaccine preparation with particular reference to the application of binary ethylenimine, Vaccine 8 (1990) 299–303.
[17] A. Sarkar, R.P. Tamil Selvan, S. Kishore, K. Ganesh, V. Bhanuprakash, Comparison of different inactivation methods on the stability of Indian vaccine strains of foot and mouth disease virus, Biologicals 48 (2017) 10–23.
[18] S. De Flora, G. Badolati, Thermal inactivation of untreated and gamma-irradiated A2-Aichi-2-68 influenza virus, J. Gen. Virol. 20 (1973) 261–265.
[19] D. Scheidegger, R.P. Pecora, P.M. Radici, S.C. Kivatinitz, Protein oxidative changes in whole and skim milk after ultraviolet or fluorescent light exposure, J. Dairy Sci. 93 (2010) 5101–5109.
[20] J. Glaeser, A.M. Nuss, B.A. Berghoff, G. Klug, Singlet oxygen stress in microorganisms, Adv. Microb. Physiol. 58 (2011) 141–173.
[21] C. Triantaphylides, M. Havaux, Singlet oxygen in plants: production, detoxification and signaling, Trends Plant Sci. 14 (2009) 219–228.
[22] A.W. Girotti, T. Kriska, Role of lipid hydroperoxides in photo-oxidative stress signaling, Antioxidants Redox Signal. 6 (2004) 301–310.
[23] M.J. Mueller, S. Berger, Reactive electrophilic oxylipins: pattern recognition and signalling, Phytochemistry 70 (2009) 1511–1521.
[24] C.P. Stanley, G.J. Maghzal, A. Ayer, J. Talib, A.M. Giltrap, S. Shengule, K. Wolhuter, Y. Wang, P. Chadha, C. Suarna, O. Prysyazhna, J. Scotcher, L.L. Dunn, F.M. Prado, N. Nguyen, J.O. Odiba, J.B. Baell, J.P. Stasch, Y. Yamamoto, P. Di Mascio, P. Eaton, R.J. Payne, R. Stocker, Singlet molecular oxygen regulates vascular tone and blood pressure in inflammation, Nature 566 (2019) 548–552.
[25] B. Li, L. Lin, H. Lin, B.C. Wilson, Photosensitized singlet oxygen generation and detection: recent advances and future perspectives in cancer photodynamic therapy, J. Biophot. 9 (2016) 1314–1325.
[26] N. Watabe, Y. Ishida, A. Ochiai, Y. Tokuoka, N. Kawashima, Oxidation decomposition of unsaturated fatty acids by singlet oxygen in phospholipid bilayer membranes, J. Oleo Sci. 56 (2007) 73–80.
[27] M.C. Wolf, A.N. Freiberg, T. Zhang, Z. Akyol-Ataman, A. Grock, P.W. Hong, J. Li, N.F. Watson, A.Q. Fang, H.C. Aguilar, M. Porotto, A.N. Honko, R. Damoiseaux, J.P. Miller, S.E. Woodson, S. Chantasirivisal, V. Fontanes, O.A. Negrete, P. Krogstad, A. Dasgupta, A. Moscona, L.E. Hensley, S.P. Whelan, K.F. Faull, M.R. Holbrook, M.E. Jung, B. Lee, A broad-spectrum antiviral targeting entry of enveloped viruses, Proc. Natl. Acad. Sci. U. S. A. 107 (2010) 3157–3162.
[28] F. Vigant, J. Lee, A. Hollmann, L.B. Tanner, Z. Akyol Ataman, T. Yun, G. Shui, H.C. Aguilar, D. Zhang, D. Meriwether, G. Roman-Sosa, L.R. Robinson, T.L. Juelich, H. Buczkowski, S. Chou, M.A. Castanho, M.C. Wolf, J.K. Smith, A. Banyard, M. Kielian, S. Reddy, M.R. Wenk, M. Selke, N.C. Santos, A.N. Freiberg, M.E. Jung, B. Lee, A mechanistic paradigm for broad-spectrum antivirals that target virus-cell fusion, PLoS Pathog. 9 (2013) e1003297.
[29] R.K. Plemper, Cell entry of enveloped viruses, Curr. Opin. Virol. 1 (2011) 92–100.
[30] X. Li, F. Yang, X. Hu, F. Tan, J. Qi, R. Peng, M. Wang, Y. Chai, L. Hao, J. Deng, C. Bai, J. Wang, H. Song, S. Tan, G. Lu, G.F. Gao, Y. Shi, K. Tian, Two classes of protective antibodies against Pseudorabies virus variant glycoprotein B: implications for vaccine design, PLoS Pathog. 13 (2017) e1006777.
[31] J. Wang, B. Chu, L. Du, Y. Han, X. Zhang, S. Fan, Y. Wang, G. Yang, Molecular cloning and functional characterization of porcine cyclic GMP-AMP synthase, Mol. Immunol. 65 (2015) 436–445.
[32] J. Wang, S.F. Lu, B. Wan, S.L. Ming, G.L. Li, B.Q. Su, J.Y. Liu, Y.S. Wei, G.Y. Yang, B.B. Chu, Maintenance of cyclic GMP-AMP homeostasis by ENPP1 is involved in pseudorabies virus infection, Mol. Immunol. 95 (2018) 56–63.
[33] S. Xiang, Z. Zhou, X. Hu, Y. Li, C. Zhang, J. Wang, X. Li, F. Tan, K. Tian, Complete genome sequence of a variant pseudorabies virus strain isolated in Central China, Genome Announc. 4 (2016).
[34] Y. Li, H. Chang, X. Yang, Y. Zhao, L. Chen, X. Wang, H. Liu, C. Wang, J. Zhao, Antiviral activity of porcine interferon regulatory factor 1 against swine viruses in cell culture, Viruses 7 (2015) 5908–5918.
[35] C. Wang, B. Huang, N. Kong, Q. Li, Y. Ma, Z. Li, J. Gao, C. Zhang, X. Wang, C. Liang, L. Dang, S. Xiao, Y. Mu, Q. Zhao, Y. Sun, F. Almazan, L. Enjuanes, E.M. Zhou, A novel porcine reproductive and respiratory syndrome virus vector system that stably expresses enhanced green fluorescent protein as a separate transcription unit, Vet. Res. 44 (2013) 104.
[36] S. Kim, T. Tachikawa, M. Fujitsuka, T. Majima, Far-red fluorescence probe for monitoring singlet oxygen during photodynamic therapy, J. Am. Chem. Soc. 136 (2014) 11707–11715.
[37] X. Ragas, A. Jimenez-Banzo, D. Sanchez-Garcia, X. Batllori, S. Nonell, Singlet oxygen photosensitisation by the fluorescent probe singlet oxygen sensor green, Chem. Commun. (2009), https://doi.org/10.1039/b822776d:2920-2.
[38] R.W. Redmond, J.N. Gamlin, A compilation of singlet oxygen yields from biologically relevant molecules, Photochem. Photobiol. 70 (1999) 391–475.
[39] B. Song, G. Wang, M. Tan, J. Yuan, A europium(III) complex as an efficient singlet oxygen luminescence probe, J. Am. Chem. Soc. 128 (2006) 13442–13450.
[40] H. Lin, Y. Shen, D. Chen, L. Lin, B.C. Wilson, B. Li, S. Xie, Feasibility study on quantitative measurements of singlet oxygen generation using singlet oxygen sensor green, J. Fluoresc. 23 (2013) 41–47.
[41] J. Kruk, H. Hollander-Czytko, W. Oettmeier, A. Trebst, Tocopherol as singlet oxygen scavenger in photosystem II, J. Plant Physiol. 162 (2005) 749–757.
[42] P. Di Mascio, S. Kaiser, H. Sies, Lycopene as the most efficient biological carotenoid singlet oxygen quencher, Arch. Biochem. Biophys. 274 (1989) 532–538.
[43] L.T. Lin, T.Y. Chen, S.C. Lin, C.Y. Chung, T.C. Lin, G.H. Wang, R. Anderson, C.C. Lin, C.D. Richardson, Broad-spectrum antiviral activity of chebulagic acid and punicalagin against viruses that use glycosaminoglycans for entry, BMC Microbiol. 13 (2013) 187.
[44] A.L. Bondy, R.M. Kirpes, R.L. Merzel, K.A. Pratt, M.M. Banaszak Holl, A.P. Ault, Atomic force microscopy-infrared spectroscopy of individual atmospheric aerosol particles: subdiffraction limit vibrational spectroscopy and morphological analysis, Anal. Chem. 89 (2017) 8594–8598.
[45] L.S. Shlyakhtenko, A.A. Gall, J.J. Weimer, D.D. Hawn, Y.L. Lyubchenko, Atomic force microscopy imaging of DNA covalently immobilized on a functionalized mica substrate, Biophys. J. 77 (1999) 568–576.
[46] H. Esterbauer, R.J. Schaur, H. Zollner, Chemistry and biochemistry of 4-hydroxynonenal, malonaldehyde and related aldehydes, Free Radic. Biol. Med. 11 (1991) 81–128.
[47] M. Concheiro, S.M. Simoes, O. Quintela, A. de Castro, M.J. Dias, A. Cruz, M. Lopez-Rivadulla, Fast LC-MS/MS method for the determination of amphetamine, methamphetamine, MDA, MDMA, MDEA, MBDB and PMA in urine, Forensic Sci. Int. 171 (2007) 44–51.
[48] J.R. Kanofsky, Singlet oxygen production by biological systems, Chem. Biol. Interact. 70 (1989) 1–28.
[49] C. Miry, M.B. Pensaert, Sites of virus replication in the genital organs of boars inoculated in the cavum vaginale with pseudorabies virus, Am. J. Vet. Res. 50 (1989) 345–348.
[50] S.C. MacDiarmid, Aujeszky's disease eradication in New Zealand, Aust. Vet. J. 78 (2000) 470–471.
[51] M.G. Michaels, Infectious concerns of cross-species transplantation: xenozoonoses, World J. Surg. 21 (1997) 968–974.
[52] A. Catala, Lipid peroxidation modifies the picture of membranes from the "fluid mosaic model" to the "lipid whisker model, Biochimie 94 (2012) 101–109.
[53] F. Vigant, N.C. Santos, B. Lee, Broad-spectrum antivirals against viral fusion, Nat. Rev. Microbiol. 13 (2015) 426–437.
[54] S. Scheiblhofer, J. Laimer, Y. Machado, R. Weiss, J. Thalhamer, Influence of protein fold stability on immunogenicity and its implications for vaccine design, Expert Rev. Vaccines 16 (2017) 479–489.
[55] P. Zhang, L. Lv, H. Sun, S. Li, H. Fan, X. Wang, J. Bai, P. Jiang, Identification of linear B cell epitope on gB, gC, and gE proteins of porcine pseudorabies virus using monoclonal antibodies, Vet. Microbiol. 234 (2019) 83–91.
[56] Y. Revilla, D. Perez-Nunez, J.A. Richt, African swine fever virus biology and vaccine approaches, Adv. Virus Res. 100 (2018) 41–74.